ANNALS OF GEOPHYSICS, 69, 1, NS111, 2026; doi:10.4401/ag-9402
OPEN ACCESS

3-D inversion and accuracy assessment of gravitational data to determine the depth of sedimentary layers; An Application in the Burg El-Arab Area, Northwestern Desert of Egypt

Ahmed Tarshan[1], Hassan Mohamed[*,2], Alaa Aref[1]

(1) Airborne Geophysics Department, Exploration Division, Nuclear Materials Authority, Cairo, Egypt
(2) Ground Geophysics Department, Exploration Division, Nuclear Materials Authority, Cairo, Egypt

Article history: received August 21, 2025; accepted January 26, 2026

Abstract

The study aims to determine the depth of subsurface sedimentary layers using a Fourier-based 3-D stripping inversion method and assess its accuracy. The seismic-based depth maps of the top Dabaa, Kharita, and El Alamein Formations in the Burg El-Arab Area were utilized to evaluate the inversion process's accuracy.

The calculated gravity effects of the top Dabaa, Kharita, and El Alamein Formations range were analytically estimated from thickness and density contrast and assigned to the surface observation level (Bouguer stations) before sequential stripping. The apparent density was calculated in addition to the upper and lower depth bounds of each sedimentary layer, which were used as constraints during 3-D Fourier-domain inversion procedure. The inversion results showed satisfactory fit statistics compared to seismic-based depth data. The analysis of the inversion's performance for the three inverted sedimentary layers showed that the percentage error between the inverted-based depth and the seismic-based depth was ranging from $\pm$0.004 to 21.67%. The seismic and inverted-based depths of the top Dabaa, Kharita, and El Alamein Formations were found to have correlation coefficient values of 0.88, 0.82, and 0.75, respectively.

A 2-D model was created for four horizons, including the basement layer. The 2-D modeling indicated that the study area is affected by a number of normal faults that cross most of the layers and dip into the NE and SW directions, with dipping angles ranging from 70° to 80° and 75° to 85°, respectively. The 3-D inversion results demonstrated that gravity measurements can accurately determine the depth of the sedimentary layer when stripping is performed at the Bouguer-station level and the inversion is constrained by density and seismic information, with a tolerance of up to 21.67% and decrease until it matches the true depth in some locations.

Keywords: 3-D Inversion; Terrestrial Gravity Data; Stripping Process; Apparent Density; Northwestern Desert

1. Introduction

The gravity technique is a geophysical investigation method that relies on the detection of changes in the gravity field driven by differences in the subsurface's horizontal density (Parasnis, 2012). It is a vital method for many subsurface mapping concerns and the main tool in various types of geological research (Milsom, 2003). One of the most significant tasks of gravity is the study of deep structures. By eliminating the top layer of the subsurface, it is possible to magnify the anomaly of deeper subsurface gravity sources (Hammer, 1963).

The 'forward problem' is regarded as a direct problem in applied geophysics, and it is always uniquely solved, in which a model is provided and data is estimated. In the "inverse problem, the scenario is usually inverted; measurements are obtained, and a plausible and data-compatible layered-earth model is produced. The inverse problem in the gravity technique is the task of producing density interfaces from observable data. These interfaces are statistically dependent because virtually all field data are ambiguous due to the inherent non-uniqueness of potential-field inversion (Blakely, 1995; Lines and Treitel, 1984; Webring, 1985).

Because the observed data and the needed model parameters (layer density and depth) are invariably non-linear, an iterative technique is commonly utilized where the non-linear inverse problem is substituted by its linearised approximation to be addressed at each iteration. As a result, the purpose of the inversion is to minimise the divergence between the estimated and observed values. The response function is expanded into a Taylor's series approximation in order to linearise it around an initial model (initial guess) and create an iterative inversion strategy (Lines and Treitel, 1984; Webring, 1985; Menke, 2012; Habeeb et al., 2017).

The traditional "Gauss-Newton" method (Lines and Treitel, 1984; Webring, 1985; Menke, 2012) can be used to progressively improve (fine-tune) the original model until an optimal model is achieved in a suitable least-squares sense. As a result, the technique is repeated until a certain convergence threshold is reached. The standard weighted least-squares criteria (chi-square (Chi^2) or root mean-square (RMS) misfit) are used to assess the accuracy with which the model fits the observed data, with the main objective of reducing the well-known estimate (Habeeb et al., 2017).

A starting (initial) model with the number of layers is needed. Prior information is used to constrain the solution by repeatedly adjusting the layer thicknesses and physical properties to best fit the data within a certain tolerance (Menke, 2012; Habeeb et al., 2017).

Layered-earth inversion can be done in the spatial or frequency domain. Spatial-domain techniques (Bott, 1963; Danes, 1960; Corbató, 1965; Tanner, 1967; Barbosa et al., 1999) are inherently more flexible than frequency-domain techniques and are easier to use for inversion schemes. However, frequency-domain inversion, which uses the sum of the Fast Fourier transform (FFT) of the gravitational anomaly (Parker, 1973; Oldenburg, 1974; Pilkington and Crossley, 1986), takes more computational time than spatial-domain techniques, especially when the earth model is large or non-uniform. However, a spectral inversion represents the summation of the sine and cosine series over a limited number of discrete wavelengths with fixed gridded data and uniform spacing. Therefore, the associated computations are more efficient, accurate, and require a minimal number of assumptions.

The Western Desert represents two-thirds of Egypt. The Northwestern Desert is a significant source of oil and gas in Egypt and is represented by three major provinces: the Northwestern Desert, the Nile Delta, and the Gulf of Suez (Kamal et al., 2023). The study area (Fig. 1) is located in the Northwestern Desert of Egypt between longitude 29°35′03.07″ to 30°03′06.32″ and latitude 30°43′15.08″ to 30°54′35.22″.

Some research was conducted in the area surrounding the study area. Ismail et al. (2015) determined the location, extent, orientation, and depth of subsurface structures in the El Alamein area in the Western Desert. They used gravity and airborne magnetic data to accomplish this goal. To distinguish the residual components from the regional components, the fast Fourier transform method was employed. The generated maps demonstrated that the E-W, NE-SW, and NW-SE tectonic trends mostly impacted the area. The study used 3-D Euler deconvolution to detect magnetic edges and create a basement structural map. It also applied 2-D modelling to gravity and magnetic profiles. The study found that the Conrad discontinuity's depth decreased from 20.5 km in the southern part to 17.9 km in the northern part, and the Moho discontinuity's depth varied from 31.5 to 28.5 km.

Saada and El-Khadragy (2015) identified the tectonic setting and structure of the basement layer in West El-Minya in the Egyptian Western Desert. They used least-squares polynomial fitting and the filtering analysis approach to identify the main subsurface tectonic trends. Bouguer gravity and magnetic anomalies maps, as well as drilled wells, were used to construct models of the Earth's crust along four profiles spanning in different directions. The top crust was separated into two sections by these models: the upper section is composed of a variety of blocks with various densities and magnetic susceptibilities, while the lower section is devoid of magnetic susceptibilities. They found

that the Moho discontinuity's depth spans from 30.5 to 34.9 km, whereas the Conrad discontinuity's depth ranges from 21.2 to 24.7 km. The basement's depth spans from 0.5 to 4.2 km, according to the basement relief map created using the computed depths.

Elmasry et al. (2022) studied the Abu Gharadig Basin, the second-most significant reservoir for hydrocarbon production in Egypt. The essential target of the study was to examine the geothermal resources using temperature well data, gravity, and airborne magnetic surveys. Using 3-D gravity inversion, the basement layer was determined, and spectral analysis of the airborne magnetic data was used to determine the Curie Point Depths (CPDs). They came to the conclusion that the CPDs extend from 17 to 22 km, and the depth to the basement rocks is between 4.5 and 7 km. Furthermore, the range of the computed heat flow values is 52-86 mW/m^2, whereas the predicted thermal gradients range from 25 to 34 °C per kilometre.

Kamal et al. (2023) evaluated the dominating structures and how they related to the basin structure in the Egyptian Western Desert. They interpreted the aeromagnetic and aerogravity results qualitatively. They came to the conclusion that the subsurface structural elements are trending in the N-S, E-W, NE-SW, and NW-SE directions. The basement's structural orientation is NE-SW and N-S, with 44 faults. In addition, the best Euler depth deconvolution identified Sill, Dyke, and Step structures.

The primary objective of this study is to assess the precision of measured terrestrial gravity data in estimating the depth of the subsurface sedimentary layers. The procedure entails: 1) analysing the obtained processed terrestrial gravity data of the study area through applying filtering techniques and edge detection; 2) estimating the gravity effect at three separate levels: the top Dabaa, the top Kharita, and the top El Alamein Formations; 3) performing stripping techniques on the Bouguer gravity data; 4) estimating the lateral density distribution at the three specified layers; 5) applying 3-D depth inversion to the tops of the Dabaa, Kharita, and El Alamein Formations; and 6) evaluating the inversion accuracy statistically using interpreted seismic depth maps.

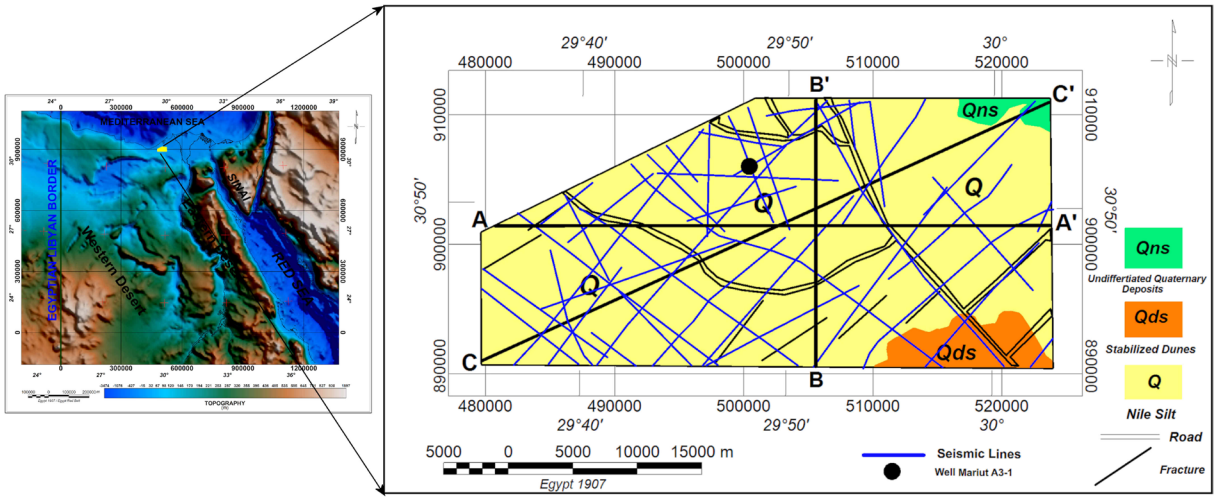

Figure 1. Location (left) and surface geological map (right) of the study area, showing seismic lines and well locations (modified after Conoco, 1987).

2. Geological setting

The Western Desert is mostly made up of a flat plateau with a few depressions and oases (Elmasry et al., 2022). Because of the lateral movements between the African and European plates, the Egyptian Western Desert may be structurally split into three primary provinces that developed along areas of weakness over the whole African plate (Mansour et al., 2020). According to Said (1990), the Northwestern Desert is primarily distinguished by relatively moderate subsidence that occurs close to active subsidence basins or depocentres. The most significant tectonic event, according to the Northwestern Desert, is thought to have occurred between the late Cretaceous and early Tertiary. This region is part of Egypt's tectonic framework's unstable band. The Western Desert's primary structural features are in the NE to ENE, E to W, and WNW to NW directions (Meshref, 1990).

Deformed sequences of sedimentary rocks are a common feature of numerous basins in the Western Desert, due to several cycles of marine incursion associated with at least three orogenic processes (Awad, 1984; Said, 1990). The Caledonian orogeny, which occurred in the middle Paleozoic, was the first of these processes. The second Hercynian orogeny movement, which occurred at the end of the Paleozoic, followed it. During the Jurassic and Tertiary periods, a third movement known as the Alpine orogeny occurred. These orogenic periods were in charge of the Western Desert's sedimentary basins and also influenced how they were oriented (Kamal et al., 2023).

The lithostratigraphic column (Fig. 2) of the Northwestern Desert includes many rock groups ranging from the Precambrian to recent deposits. The basement of the Precambrian, which is mostly found in the deeply drilled wells,

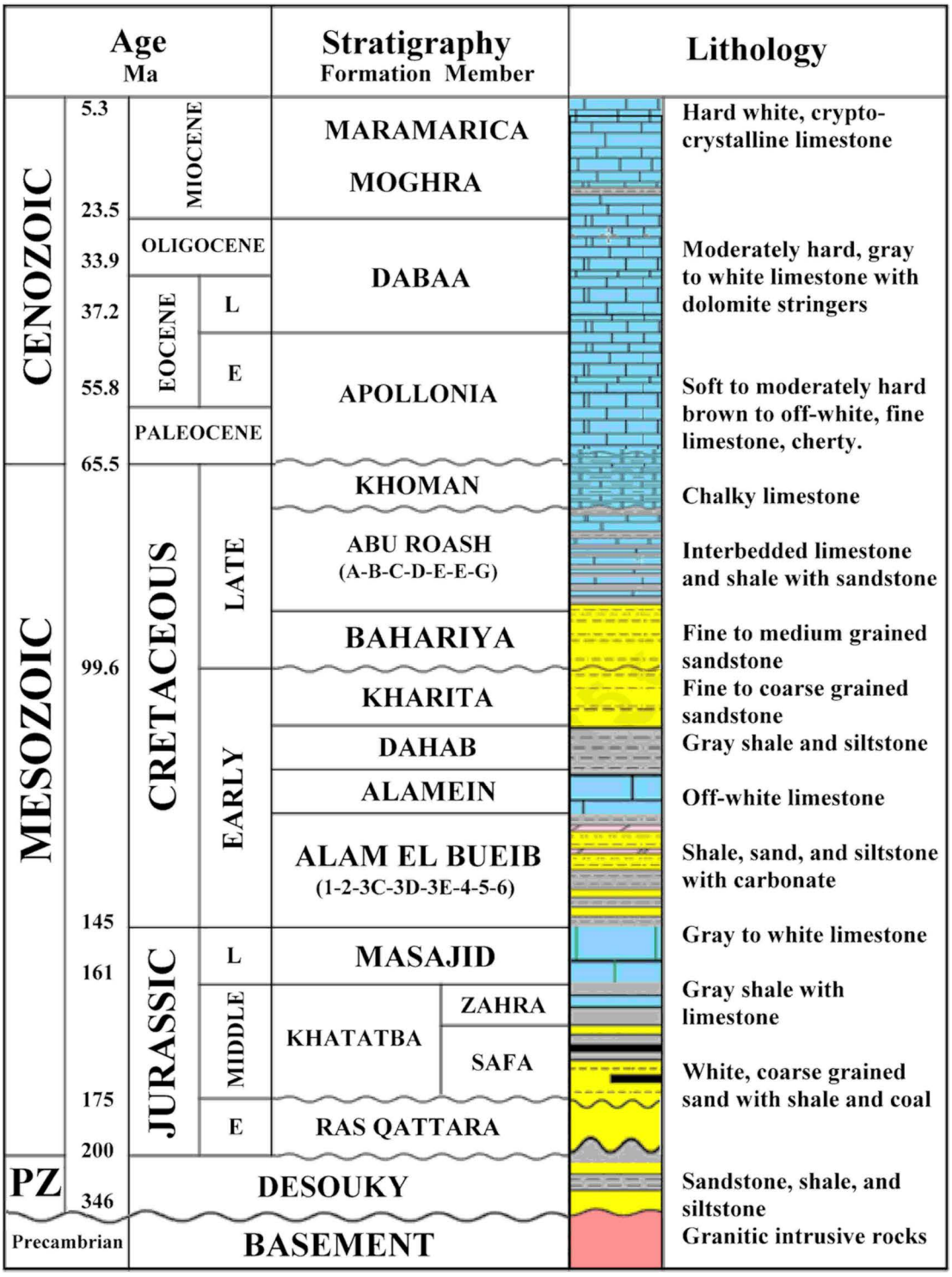

Figure 2. Litho-stratigraphic column of the Northwestern Desert of Egypt (Bosworth et al., 2015).

rests irregularly on the earliest Paleozoic strata. The depth to the basement in these basins is determined using potential field data from the Western Desert (Saada and El-Khadragy, 2015; Saada et al., 2022). According to Said (1962), the geologic section is made up of clastic cycles and alterable sedimentary carbonates. Paleozoic deposits in the Northwestern Desert were created by the interbedding of shale and sandstone, as well as a few small carbonate layers.

The Desouky Formation's pre-rift strata (Fig. 2) were deposited in the Paleozoic. The majority of continental rift basin sedimentary sequences start with fluvial sandstones (Lower Jurassic Ras Qattara Formation). The Paleozoic and Mesozoic periods are separated by a significant unconformity (Abd El Gawad et al., 2016; Edress et al., 2022).

The Khatatba Formation's syn-rift deposits are a result of early Jurassic rifting. It may be separated into two members: the Zahra shale and carbonate alternations and the lower Safa argillaceous sandstones. According to Taha and Halim (1992) and Moustafa (2008), these packages correspond to shallow marine to marginal marine depositional settings (Edress et al., 2022). The Khatatba Formation is Middle Jurassic in age. The Middle Jurassic back-reef facies were referred to as the "Khatatba Formation" by Norton (1967). Overall, this formation is composed of a thick carbonaceous shale pattern resulting from the interbedding of coal seams, limestone streaks, and porous sandstone (Kamal et al., 2023).

A second significant depositional cycle comprises the Lower Cretaceous Alam El Bueib, which is composed of six components (members) (Fig. 2). Carbonates alternate with argillaceous sediments to form the lower parts represented by members AEB-5 and AEB-6. These two members are followed by the AEB-4, which is composed of marine shales, followed by a sequence of fluvial sandstone divided by the marine shale of the AEB-3C member (Fagelnour et al., 2018). Following the AEB-3C member, the shale, sandstone, and carbonate of the two members (AEB-1 and AEB-2) are deposited, followed by the deposition of the El Alamein Formation's limestone and dolomite. Local shale and siltstone of the Dahab Formation were deposited to complete this cycle of deposition (Edress et al., 2022).

At the end of the Early Cretaceous, the thick fluvial Kharita Formation sediments, consisting of siltstones intercalated with fine to coarse sandstones, were deposited. This marked the start of the third major depositional cycle (Edress et al., 2022). This unit's component is always linked to a certain amount of amorphous silica (Norton, 1967).

The Late Cretaceous began with the deposition of the Baharyia Formation, which developed on a shallow sea shelf and is marked by a large unconformity. The Upper Cretaceous is depicted by the following units: 1) The Bahariya Formation stretches for at least 170 m and is split into three parts: El Heiz (upper part), Gebel Dist (middle part), and Gebel Ghorabi (lower part). 2) The Abu Roash Group, which is mostly made of limestone with interbeds of sandstone and shale (Beadnell, 1905; Kamal et al., 2023).

The end-of-late Cretaceous is indicated by the deposition of the Khoman Formation (Leeder, 2011; Edress et al., 2022). The Khoman Formation is a magnificent formation with multiple chert bands and white chalky limestone. The Cenozoic is represented by the Apollonia Formation, consisting of a limestone block deposited in the Paleocene-Middle Eocene with underlying shale components. This unit was dubbed the Apollonia Formation by Norton (1967).

The Dabaa and Moghra Formations make up the fourth cycle. The Dabaa Formation is a fairly hard, grey-to-white limestone with dolomite stringers that was deposited in the Oligocene from 33 Ma to 23 Ma. The Moghra Formation consists of limestones and shale intercalations and is overlain by Marmarica Formation limestone (Taha and Halim, 1992; Bosworth et al., 2015, Edress et al., 2022).

3. Gravity data analysis

The gravity data were collected as part of a large ground survey project conducted by the General Petroleum Company (General Petroleum Company, 2022). The Bouguer gravity data was gathered as hard copy sheets, which we then digitized for the study area, forming a Bouguer anomaly map (Fig. 3a). The study area includes 259 gravity stations that were utilized to create the Bouguer gravity map. The Bouguer values range between −2.2 and −19.4 mGal. In the study area, lower values are found in the central, eastern, and northeastern regions, whereas higher values are prominent in the western and southeast regions. Generally, increasing gravity values may be attributed to the uplift of thicker basement rock, whereas lower gravity readings are indicative of sedimentary basins. The studied region is generally characterized by negative Bouguer gravity values, which may indicate a thick sedimentary succession.

3.1 Contact Lineament Processing

The observed components of the terrestrial Bouguer gravity map (Fig. 3a) may be separated using the log power spectrum approach to analyse the data (Spector and Grant, 1970) (Fig. 3b). Separation findings should be utilized cautiously when employing the log power spectrum approach and detecting line segments since undesirable signal remnants could persist while favourable components might be diminished. Nonetheless, it can still be a useful technique to separate a field into components that approximate theoretical source depths (Feng et al., 2020).

Gravity separation was made from the Bouguer gravity anomaly map using the Gaussian filter technique. Using a band-pass filter technique with k = 0.05 km^{-1} as the cutoff parameters, the regional and residual Bouguer gravity anomaly maps (Figs. 4a and 4b) were created. The main feature of the regional map (Fig. 4a) is showing the long wavelength of the deep anomalies that have a regional trend NE-SW, which is the dominant trend in the study

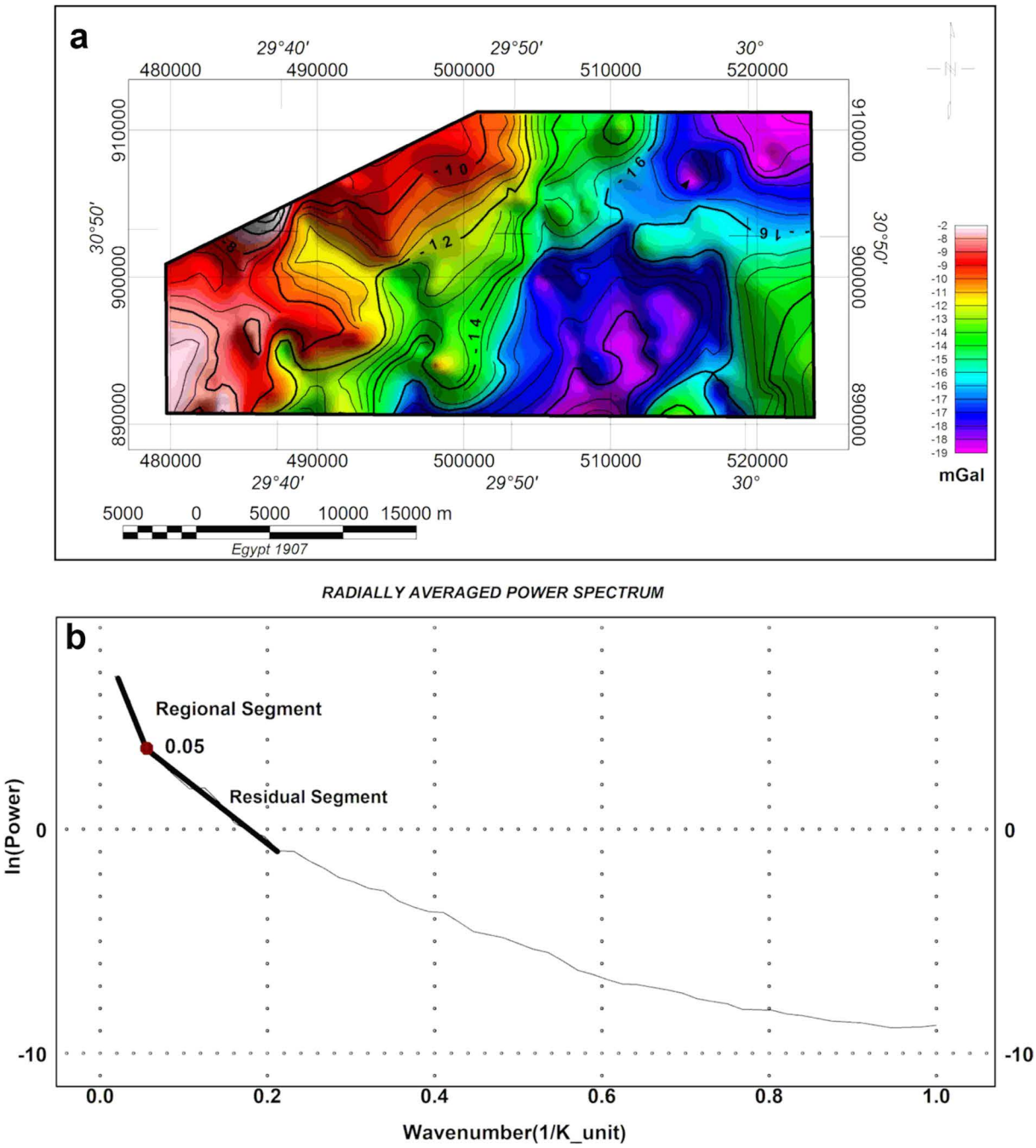

Figure 3. (a) Bouguer anomaly gravity map of the study area; (b) 2-D power spectrum of the Bouguer anomaly data.

area. The shallow anomalies are expressed by the residual map (Fig. 4b). This map is then subjected to first-vertical derivative (FVD) filtering in order to more clearly display the shallow anomalies (Fig. 5a).

The FVD approach amplifies information about short wavelengths at the expense of information about long wavelengths. Gradients along the boundaries of shallow potential field sources are highlighted on the FVD map. In order to validate sources at shallow depths and to identify the edges of potential field objects, the FVD (Fig. 5a) is utilized. Geological trends can be visualised through the study of contact lineaments. Contact lineaments (Fig. 5b) were created based on the FVD of the residual gravity anomaly component (Fig. 5a). The created rose diagram (Fig. 5b) makes it easy to determine the general trend of the lineaments. It demonstrates that the NE-SW is the major trend in the area, followed by the trends of the NNW-SEE and the NNE-SSW. In addition, another trend of lineaments is observed near the E-W direction.

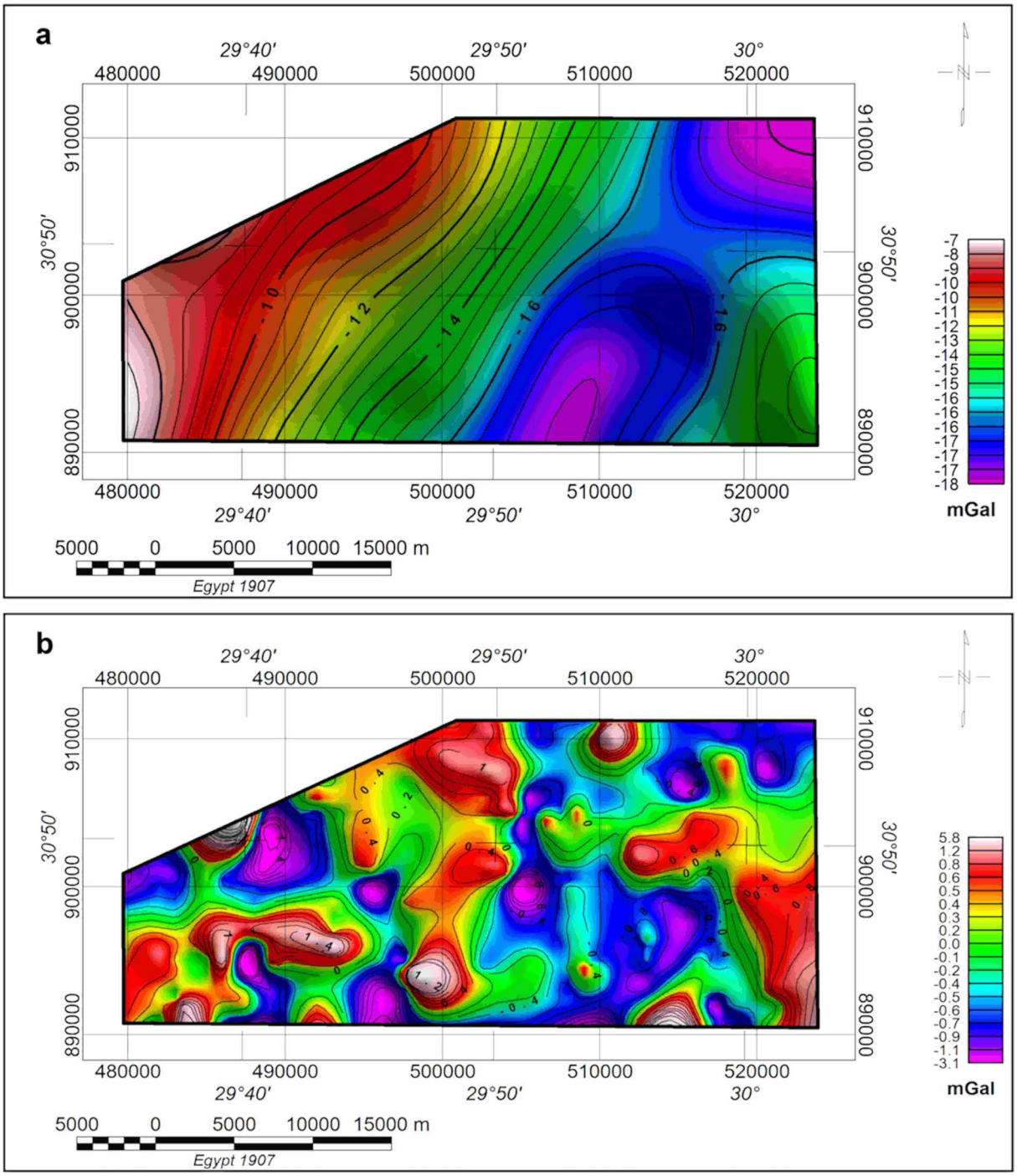

Figure 4. (a) Regional component; (b) Residual component of Bouguer gravity anomaly map.

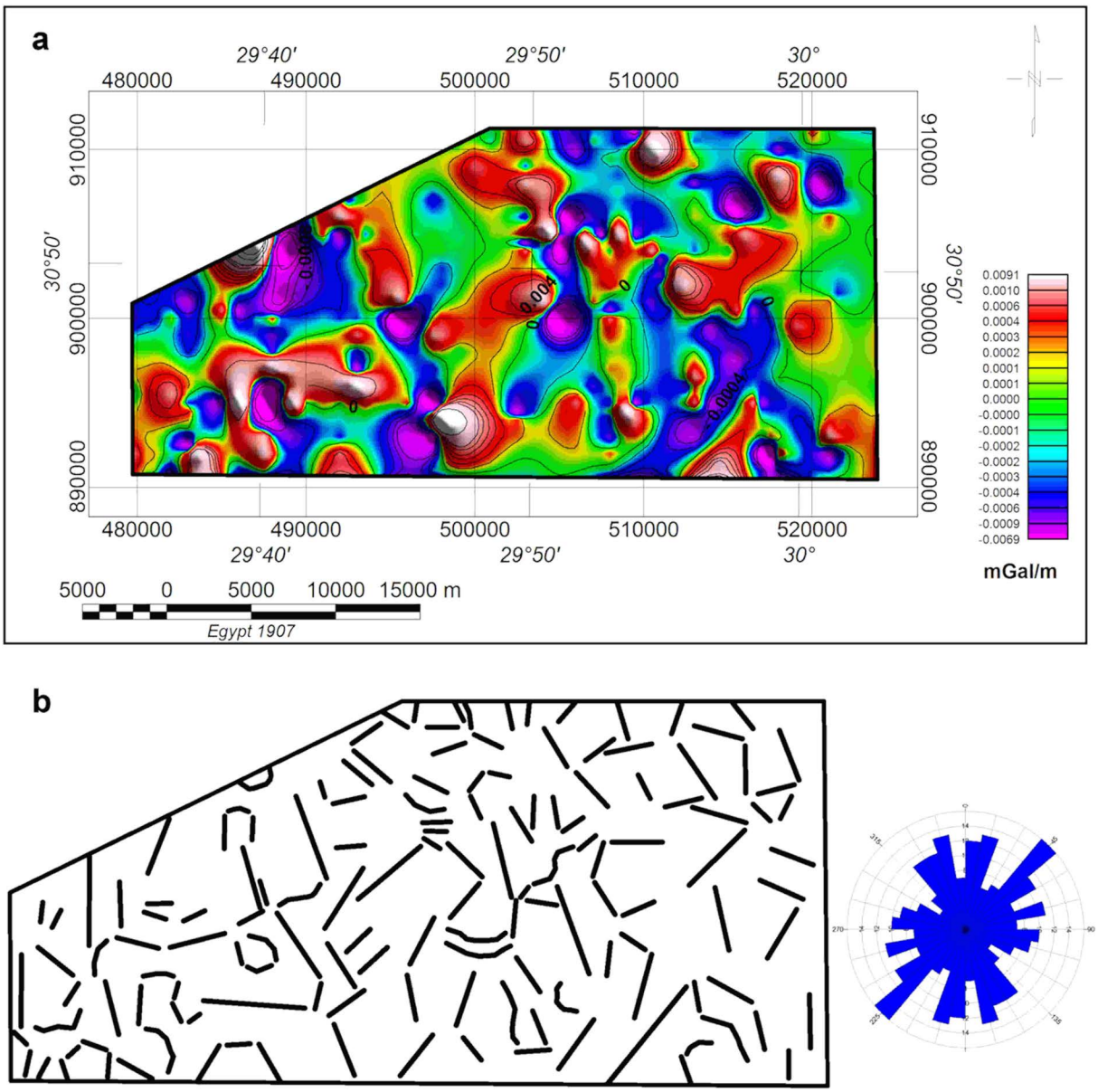

Figure 5. (a) First Vertical Derivative (FVD) of the residual Bouguer gravity anomaly map; (b) Contact lineament and Rose diagram showing the major lineament trend.

4. Methodology

Geophysical inversions are inherently ill-posed problems that lead to non-unique solutions. Therefore, there are always many models that accurately reproduce the observed data (Blakely, 1995; Tarantola, 2005; Menke, 2012; Xiao, 2020). In addition, different subsurface gravity distributions can give identical responses. It is therefore important to realise that the non-uniqueness of the inversion is largely unrelated to actual geological events and stems from the mathematical characteristics of potential fields (Blakely, 1995; Tarantola, 2005). The gravity effect of the different layers in the subsurface could be obtained from the stripping of the Bouguer gravity data.

As seen in Fig. 6, a suggested flowchart for the conducted work and inversion to estimate the depth of the sedimentary layers in the subsurface was created. Prior information about the thickness of the sedimentary layers in the study area is necessary to get reliable results, where in this research the thicknesses are derived from depth-based seismic maps. The work began by calculating the gravity effect for each selected sequence from the Bouguer gravity map (Fig. 3a). The Bouguer gravity measurements were stripped of the gravity effect to determine the gravity at the top of each selected layer, after which the apparent density for each sequence was computed. Utilizing the stripped

gravity maps, forward modelling was done. Applying constraints to the lower and upper bounds (obtained from the seismic depth maps) allowed the inversion to be applied while limiting the non-uniqueness of the process up to the convergence limit.

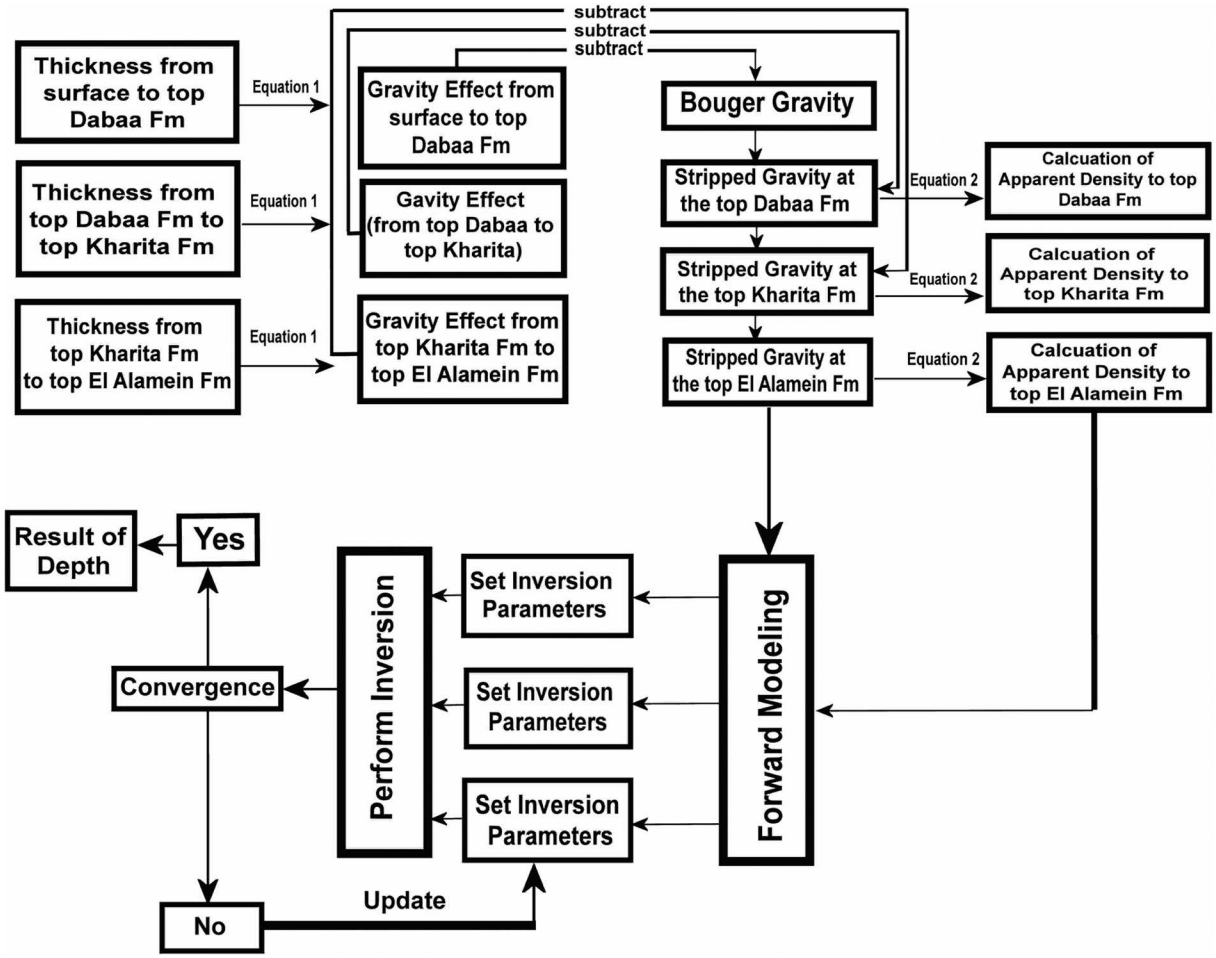

Figure 6. Proposed scheme of work and inversion to estimate the depth of sedimentary layers.

4.1 Stripping Process

4.1.1 Gravity effect calculation

The stripping process involves an assessment of the changes in thickness and density of the specified sedimentary layer to precisely calculate their gravity effects. The time-domain seismic maps of the top three sedimentary layers were obtained based on a portion of the El Paso seismic survey, the locations of which are shown in Fig. 1. Depth-domain seismic maps were obtained by the conversion of the time domain to the depth domain. In this study, the single-function time-depth curve method is used. The curve is derived from the checkshot data at Mariut A3-1 well (Fig. 7), where the x-axis is time in milliseconds and the y-axis is the depth data in meters. The time domain maps were converted to a depth domain map using the following calculated Eq. (1).

$$y = 0.0004x^2 + 6475x + 115.5431 \quad (1)$$

As a first step in calculating the effect of gravity at a given depth, the thickness of the layers is calculated. The thickness is calculated at the top of the three selected layers (Tops Dabaa, Kharita, and El Alamein Formations). These seismic-based depth maps will be used as a reference for measuring the accuracy of the inversion process later.

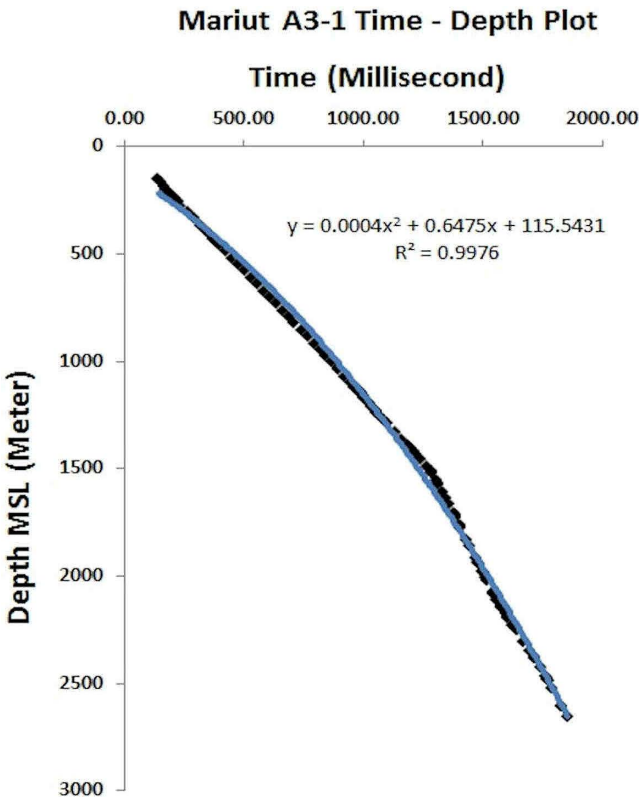

Figure 7. Time-depth plot from well Mariut A3-1.

The seismic-based depth maps of the top Dabaa, Kharita, and El Alamein Formations were used to create a series of thickness maps in order to manage the geometry at the top of each lithologic formation. The thickness maps are produced using Petrel software and then regridded using Geosoft (2008).

The thickness maps (Fig. 8) reveal that the depth to the top of the Dabaa Formation (Fig. 8a) displays a moderate thickness range between 855 and 1332 m, where the northern part is distinguished by a high thickness of sedimentary succession that continues to the middle of the area. On the opposite side, the thickness decreases, moving towards the south, reaching 855 m in the southwestern part.

The generated thickness map of the top Kharita Formation (Fig. 8b) exhibits the largest thickness of sandstone, grey shale, and limestone, reaching 1664 m in the southern part and extending to the eastern part. This thickness decreases towards the north and continues to decrease towards the northwestern part until it reaches 1067 m. The thickness from the top Kharita Formation to the top El Alamein Formation is relatively small, as the smallest thickness recorded is 28 m in the southwestern part and the largest thickness is 595 m (Fig. 8c), as the thickness increases towards the northwest of the study area.

These sets of thickness maps are utilized as a geometric control throughout the stripping process. When calculating the gravity effect, the density contrast of every rock to the basement density is determined. The determination of average density was based on inferring average density estimates from the density log of well Mariut A3-1. The average density of the limestone, which mostly forms up the succession above the top Dabaa Formation, is estimated to be 2400 kg/m^3. Sandstone intersects with carbonates, which may lead to a somewhat lower density, forming the sedimentary succession from the top Kharita to the top Dabaa Formations with an assumed average density of 2200 kg/m^3. The succession between the top Kharita and top El Alamein Formations is separated by a sequence of sandstone and shale with an expected average density equal to 2350 kg/m^3 due to the existence of shale. The Precambrian basement is assumed to have the highest density, with an average density of 2700 kg/m^3.

According to Otsuka and Ogawa (1977), the gravity effects (Δg) of the top Dabaa, the top Kharita, and the top El Alamein Formations were calculated using Eq. (2).

$$\Delta g = 2\pi G \Delta \rho h \quad (2)$$

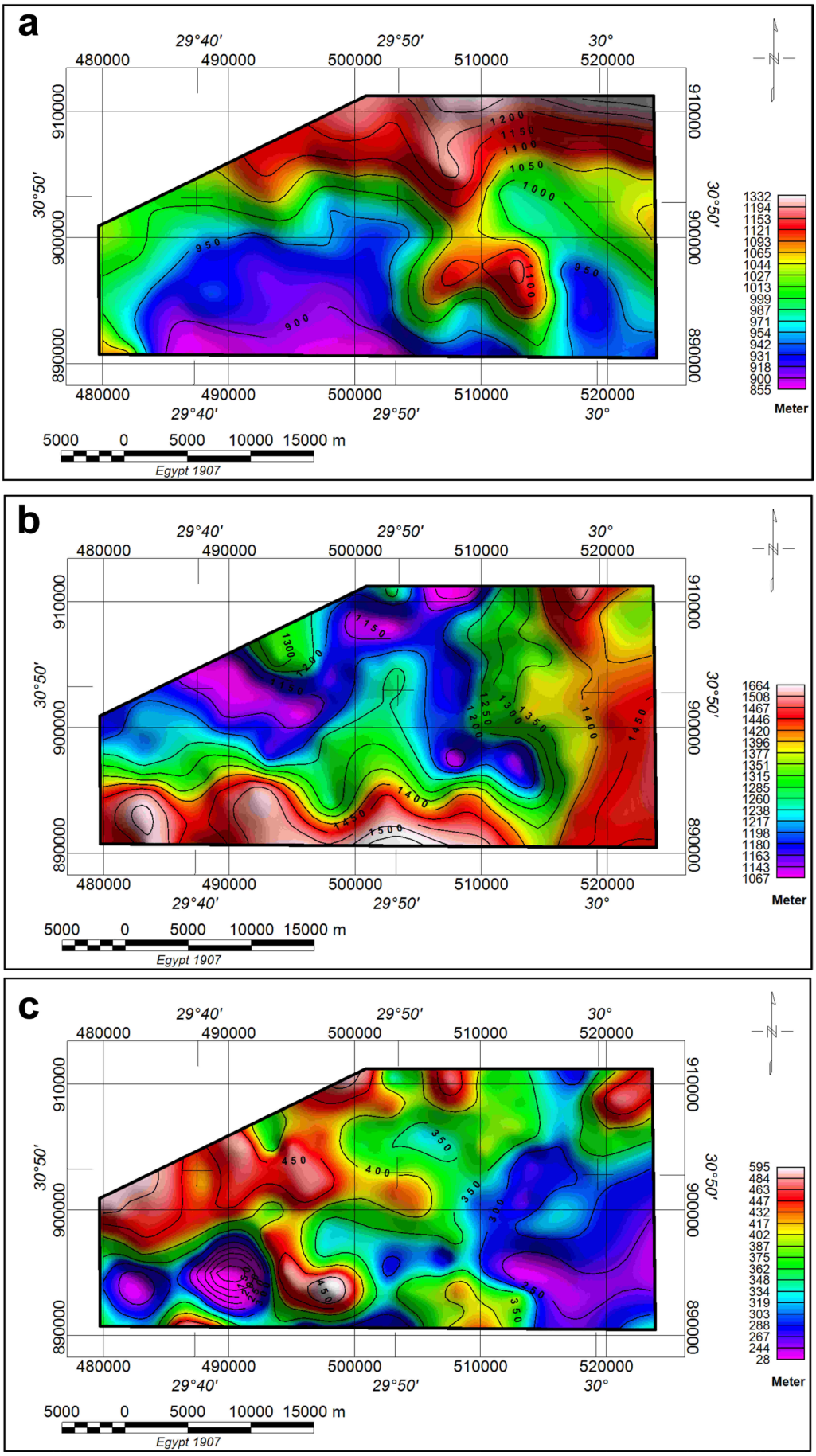

Figure 8. Thickness maps to the top: (a) Dabaa; (b) Kharita; (c) El Alamein Formations.

This equation can be written in simple form, as shown in Eq. (3).

$$\Delta g = 0.0000419 \times \text{Density contrast } (kg/m^3) \times \text{Thickness (meters)} \quad (3)$$

The gravity effect for each top formation can be calculated using Eqs. (4), (5), and (6),

$$\Delta g_{TD} = 2\pi G(\rho_{TD} - \rho_B)h_{TD} \quad (4)$$

$$\Delta g_{TK} = 2\pi G(\rho_{TK} - \rho_B)h_{TK} \quad (5)$$

$$\Delta g_{TA} = 2\pi G(\rho_{TA} - \rho_B)h_{TA} \quad (6)$$

Where,
Δg = gravity effect (mgal),
G = gravitational constant ($6.674 \times 10 - 11\ N{\cdot}m^2/kg^2$),
ρ_{TD}, ρ_{TK}, ρ_{TA} and ρ_B = densities (kg/m^3) of the top Dabaa, top Kharita, top El Alamein, and basement formations, respectively,
TD = top Dabaa,
TK = top Kharita,
TA = top El Alamein,
B = basement,
h = thickness of layers (m).

The gravity effects of the Dabaa, Kharita, and El Alamein Formations were computed analytically from the mapped layer thicknesses and density contrasts using the slab relations in Eqs. (2-6). These analytical estimates represent a first-order physical approximation of how density contrast ($\Delta\rho$) and layer thickness (h) contribute to the gravity field. All layer-effect values were evaluated directly at the surface observation level (Bouguer stations) to ensure consistency with the measured Bouguer anomaly during the stripping procedure.

These analytical layer-effect grids were used only to perform the sequential stripping (Eqs. 7-9). The subsequent inversion of the stripped gravity fields was carried out using the 3-D Fourier-domain algorithm implemented in GMSYS-3D, following Parker (1973), Oldenburg (1974), and Pilkington and Crossley (1986), which provides the final depth solutions.

The amplitudes of the analytically estimated layer effects (−28 to −18 mGal for Dabaa; −21 to −13 mGal for Kharita; −9 to −0.4 mGal for El Alamein) are consistent with the magnitude and wavelength of the measured Bouguer anomaly, confirming the physical plausibility of the approach. In this work, the expression 'at the top of each formation' refers to the stratigraphic level used for sequential stripping, rather than the computational depth of the gravity field.

4.1.2 Stripped gravity calculation

The Bouguer gravity data and the analytically computed layer-effect grids, derived from Eqs. (2-6) and assigned to the surface observation nodes (Bouguer station level), were used to obtain the stripped gravity field. Stripping was then applied sequentially at the Bouguer station level according to Eqs. (7-9).

$$\Delta g_{strip(TD)} = \Delta g_{boug} - \Delta g_{TD} \quad (7)$$

$$\Delta g_{strip(TK)} = \Delta g_{Strip(TD)} - \Delta g_{TK} \quad (8)$$

$$\Delta g_{strip(TA)} = \Delta g_{Strip(TK)} - \Delta g_{TA} \quad (9)$$

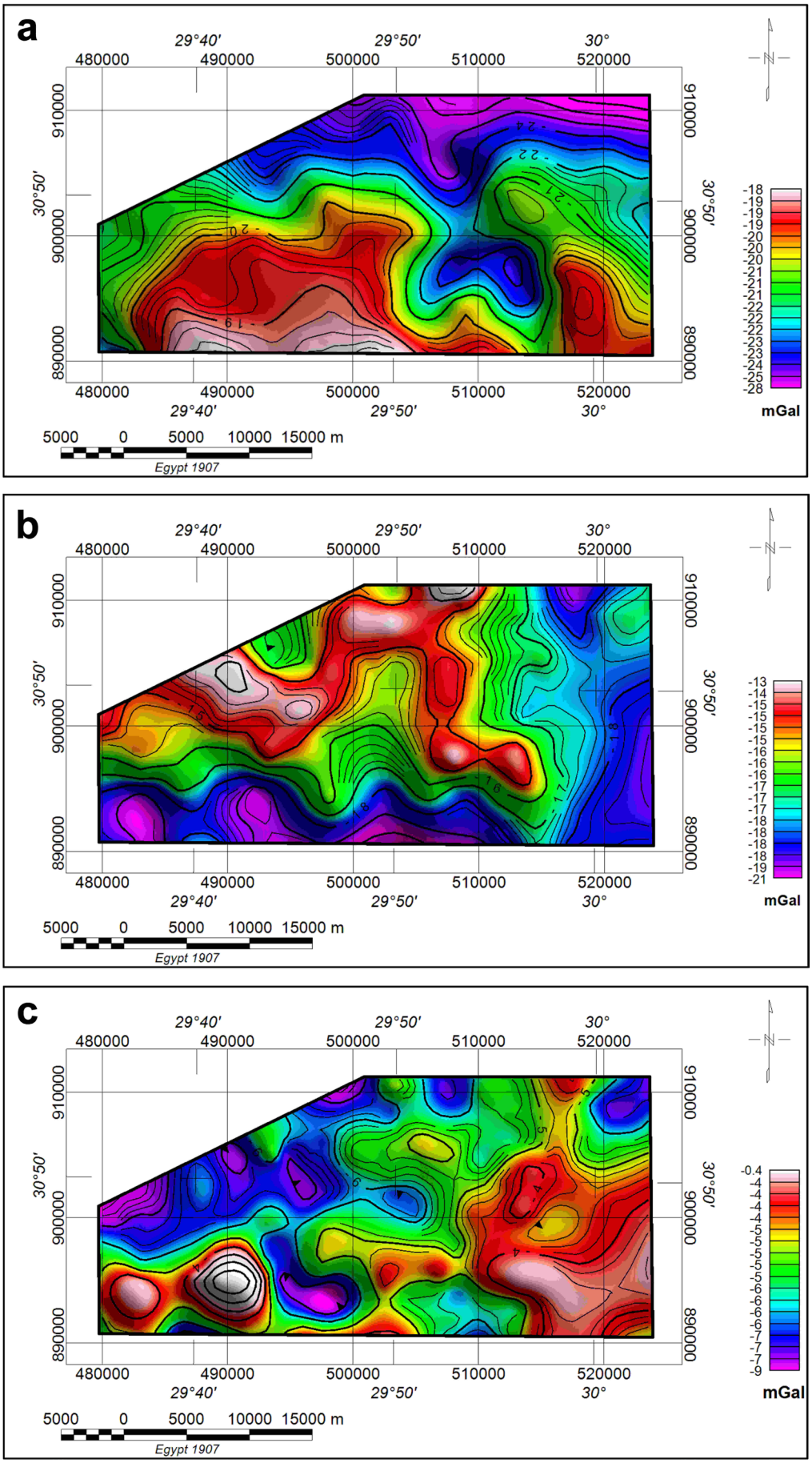

Figure 9. Gravity effect maps of the top (a) Dabaa; (b) Kharita; (c) El Alamein Fotmations.

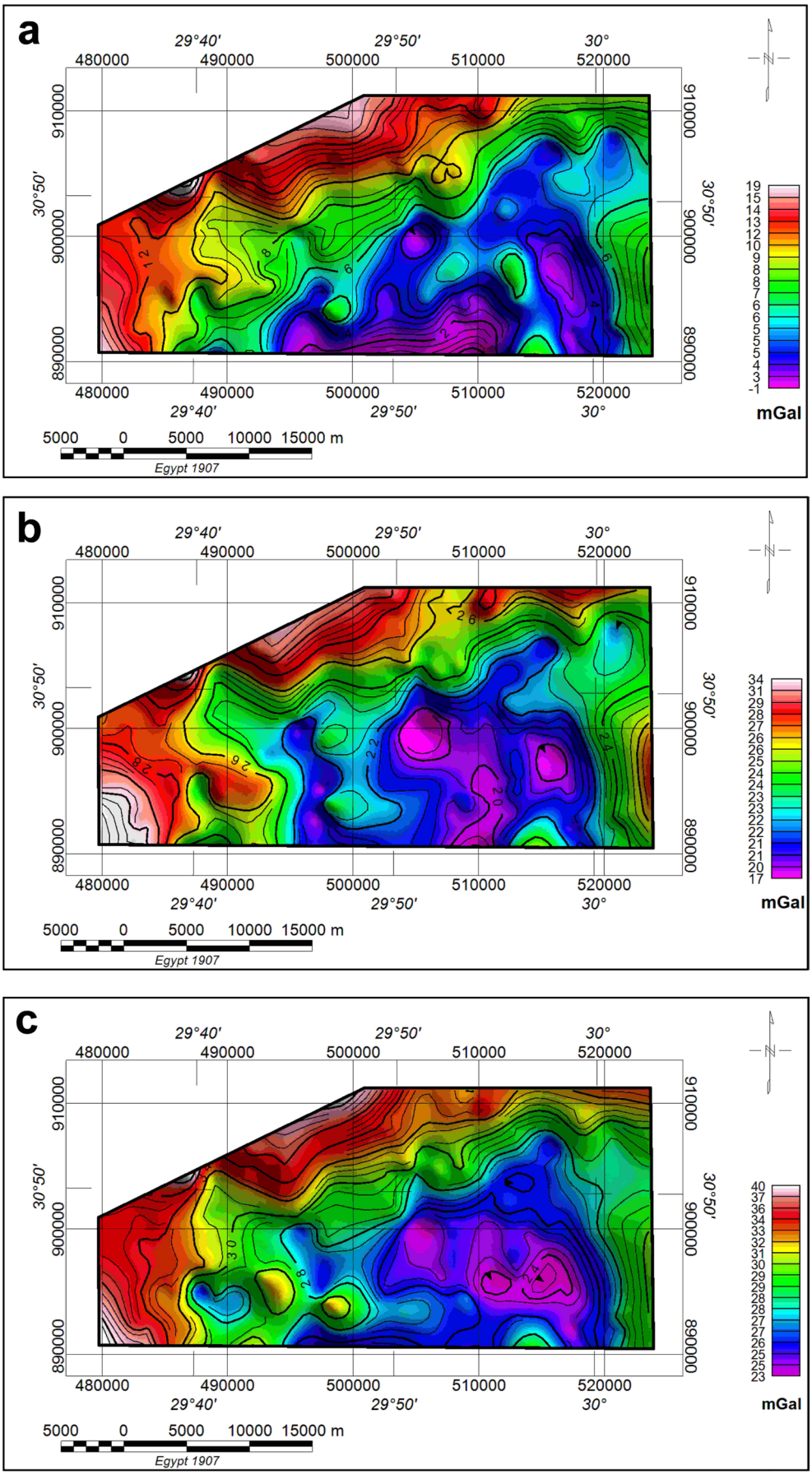

Figure 10. Stripped gravity maps referenced to the surface observation level for the tops of: (a) Dabaa; (b) Kharita; (c) El Alamein Formations.

Where,
$\Delta g_{strip(TD)}$: gravity anomaly after stripping at the top Dabaa Formation,
$\Delta g_{strip(TK)}$: gravity anomaly after stripping at the top Kharita Formation,
$\Delta g_{strip(TA)}$: gravity anomaly after stripping at the top El Alamein Formation,
Δg_{boug}: gravity anomaly before stripping,
Δg_{TD}: gravity effect at the top Dabaa Formation,
Δg_{TK}: gravity effect at the top Kharita Formation,
Δg_{TA} gravity effect at the top El Alamein Formation.

Using Eq. (7), the stripped gravity map for the Dabaa Formation was calculated (Fig. 10a). The top Kharita Formation's stripped gravity was then created by subtracting the gravity effect of the Kharita Formation from it (Fig. 10b). Consequently, the gravity effect of the top El Alamein Formation was subtracted from the stripped gravity for the Kharita Formation to obtain the stripped gravity map for the El Alamein Formation (Fig. 10c). The stripped gravity maps (Fig. 10) and the Bouguer gravity map (Fig. 3a) show comparable spatial patterns in anomaly distribution, confirming that all stripping computations were performed at the surface observation level, ensuring consistency with the measured gravity data.

4.2 3-D Depth inversion estimation

Depths were calculated using 3-D Fourier-domain inversion in GMSYS-3D (following Parker, 1973; Oldenburg, 1974; Pilkington and Crossley, 1986), with apparent-density constraints derived from the stripped-gravity maps. The inversion was driven by the stripped-gravity maps (Fig. 10), which provide the residual gravity field after sequential removal of analytically estimated layer effects, all referenced to the surface observation level (Bouguer stations).

For each formation, the apparent lateral-density distribution was computed from the stripped-gravity field and used as a spatial constraint to stabilize the inversion and reduce non-uniqueness. These apparent-density grids guide the inversion toward geologically plausible depth solutions, consistent with the independent seismic-based depth information.

4.2.1 Density estimation

Due to the lack of information about the variation of density in the study area, the apparent lateral-density distribution was calculated based on the stripped gravity values at the three top formations, which can be used as a constraint to control the inversion process for each layer.

Apparent density mapping presupposes a simple model layer with variable density and constant thickness to describe the measured gravitational field. The calculated response is assumed to be driven by an array of square-ended vertical prisms with an infinite depth extent; dimensions horizontally are the same as the input grid cell size (Blakely, 1995).

Although the apparent density model does not take into account the morphology of the rock discontinuity, assuming it is flat, it attributes the effects of anomalies entirely to density variations. In principle, apparent densities can be converted to morphological variations of the layers, but at least a priori information about the maximum and minimum source depths must be assumed. Information about the maximum and minimum depths was obtained from seismic-based depth maps, and a reference density value was obtained from the density log of the Mariut A3-1 well.

Using Eq. (10), as implemented in the GMSYS-3D apparent-density module and derived from the Fourier-domain formulations of Parker (1973), Oldenburg (1974) and Pilkington and Crossley (1986), the apparent density to the top Dabaa, Kharita, and El Alamein Formations is calculated.

$$L(r) = r/2\pi G\left(1 - e^{(-tr)}\right), \tag{10}$$

Where
$L(r)$: apparent density (kg/m^3)

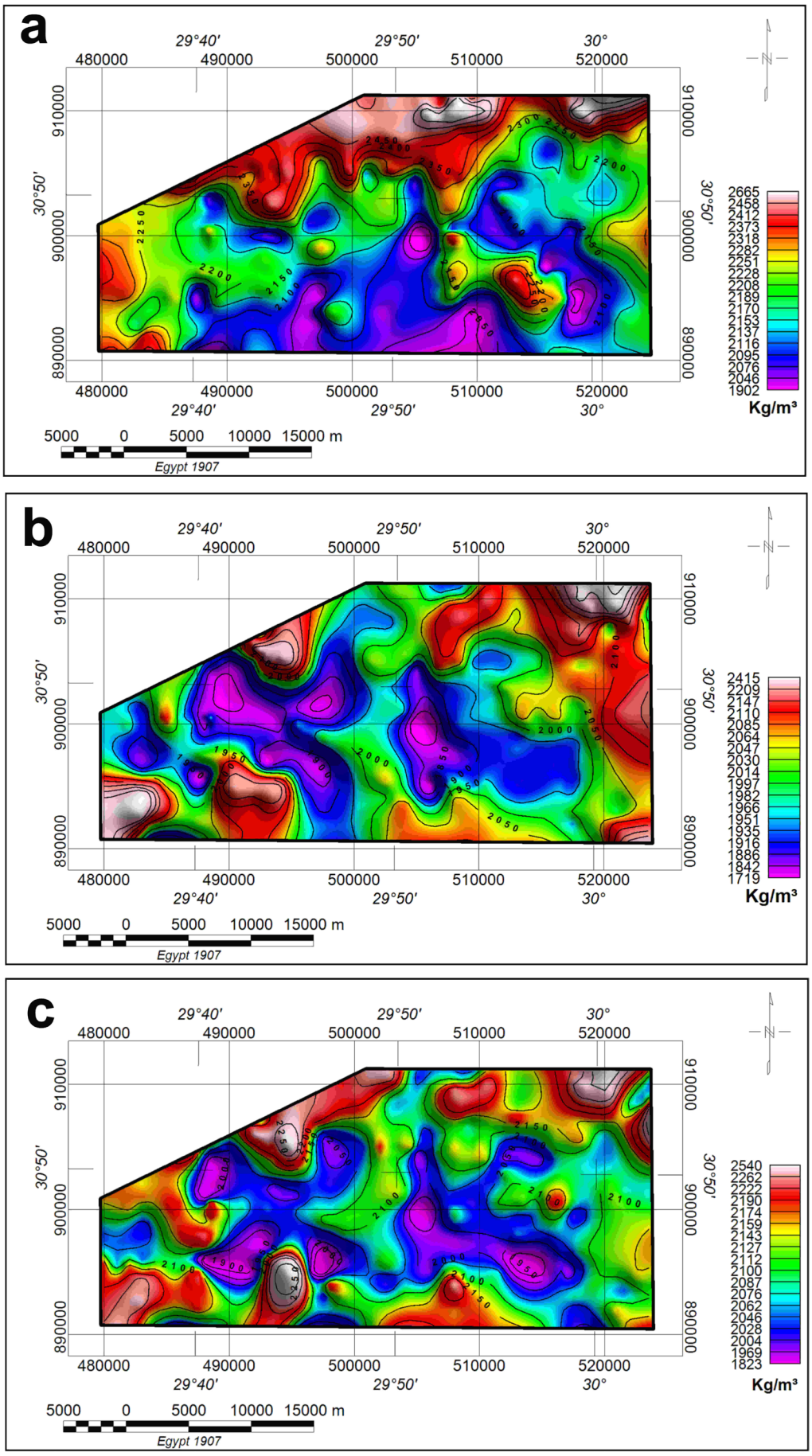

Figure 11. Apparent lateral density distribution of the top: (a) Dabaa; (b) Kharita; (c) El Alamein Formations.

r: wavenumber (radians/ground_unit)
t: thickness, in ground units, of the earth model.

The estimated apparent density of the top Dabaa Formation (Fig. 11a) ranges from about 1902 to 2665 kg/m^3. The area's northern part has the highest density values, which decrease to the south. The top Kharita Formation's apparent density map (Fig. 11b) shows a range of values from 1719 to 2415 kg/m^3, where the higher values clustered along the study area's boundaries and the lower values in the central part. The El Alamein Formation's apparent density map (Fig. 11c) has values ranging from 1823 to 2540 kg/m^3, where the central part has the lowest values.

4.2.2 3-D Inverse modeling

In geophysics, several inversion approaches are now in use; one of the most well-known is Parker's method (Parker, 1973), which is based on an iterative process employing Fourier transforms to find the underlying density distribution. This technique is simplified by modeling the anomaly field sources with some help from the geological knowledge available in the survey region. The current gravity data inversion aims to detect the depth to the top Dabaa, Kharita, and El Alamein Formations.

A model is represented by a series of packed surface grids, each with its own lateral density distribution allocated to the layer underlying each surface. Parker's method (Parker, 1973) using GMSYS-3D, a 3-D gravity modeling tool for surface-oriented models, was used for the calculations, which were done in the wave number domain. Geosoft (2008) developed the program in order to make use of all the grid manipulation and display options. The constraint to minimize non-uniqueness and instability is often compensated by creating an inversion function guided by prior information (Feng et al., 2020). Therefore, for every inverted layer, the calculated apparent lateral density distribution has been utilized as a constraint for each layer.

Because GMSYS-3D employs frequency-domain calculation procedures, the grids must be carefully prepared to work with FFT. There can be no dummies in the grid, no crossing surfaces, and all the grids in the model must have the same grid size (number of rows and columns), cell size, and units. All grids are referenced to a reference index grid.

All grids must be expanded and "filled" to make them "periodic" to eliminate edge effects. For all grids, the expansion was set at 30%. The final expanded dimensions of the grid must also be "good FFT" dimensions. A smooth interpolation is then used to wrap the grid from one edge of the "real data" off the edge of the expanded grid and back from the other side of the expanded grid to the "real data" on the other side. This process is done regularly for all expanded grids.

Structural inversion based on gravity misfit in each horizon is performed separately for each selected layer. The lateral density distribution maps (Fig. 11) of each layer were set as a constraint for the inversion process. A depth layer with fixed values is set as input, with a fixed value for each layer. The initial depth layers were established for the top Dabaa, Kharita, and El Alamein Formations at average values of –900, –2000, and –2450 m, respectively. A set of parameters is adjusted to control the accuracy of the inversion process. These parameters include a 0.1 mGal convergence limit used to achieve good convergence between measured and estimated gravity anomaly data. The convergence limit is reached after several iterations equal to 8 for the top Dabaa, 6 for the top Kharita, and 10 for the top El Alamein. The mean misfit error between the observed and calculated gravity data was found to be ±0.058 mGal for the top Dabaa Formation. The mean misfit for the Kharita and El Alamein Formations is equal to ±0.009 and ±0.201 mGal, respectively.

5. Results and Discussion

The findings of the inversion of the terrestrial gravity data show good agreement with the seismic-based depth maps. The constructed seismic-based depth map (Fig. 12a) of the top Dabaa Formation ranges from 855 to 1332 m; a sufficient similarity with the inverted depth is observed. The inverted depth map of the top Dabaa Formation (Fig. 12b) ranges from 759 to 1230 m. The northern part shows high depth values ranging from 1116 to 1230 m, where these values decrease to the south, reaching 759 m in the southwest. In spite of this similarity between the two maps, some differences appear in the central part of the study area, where some anomalies appear at shallower depths in the inverted depth map than in the seismic-based depth map. The range of the difference between the two maps

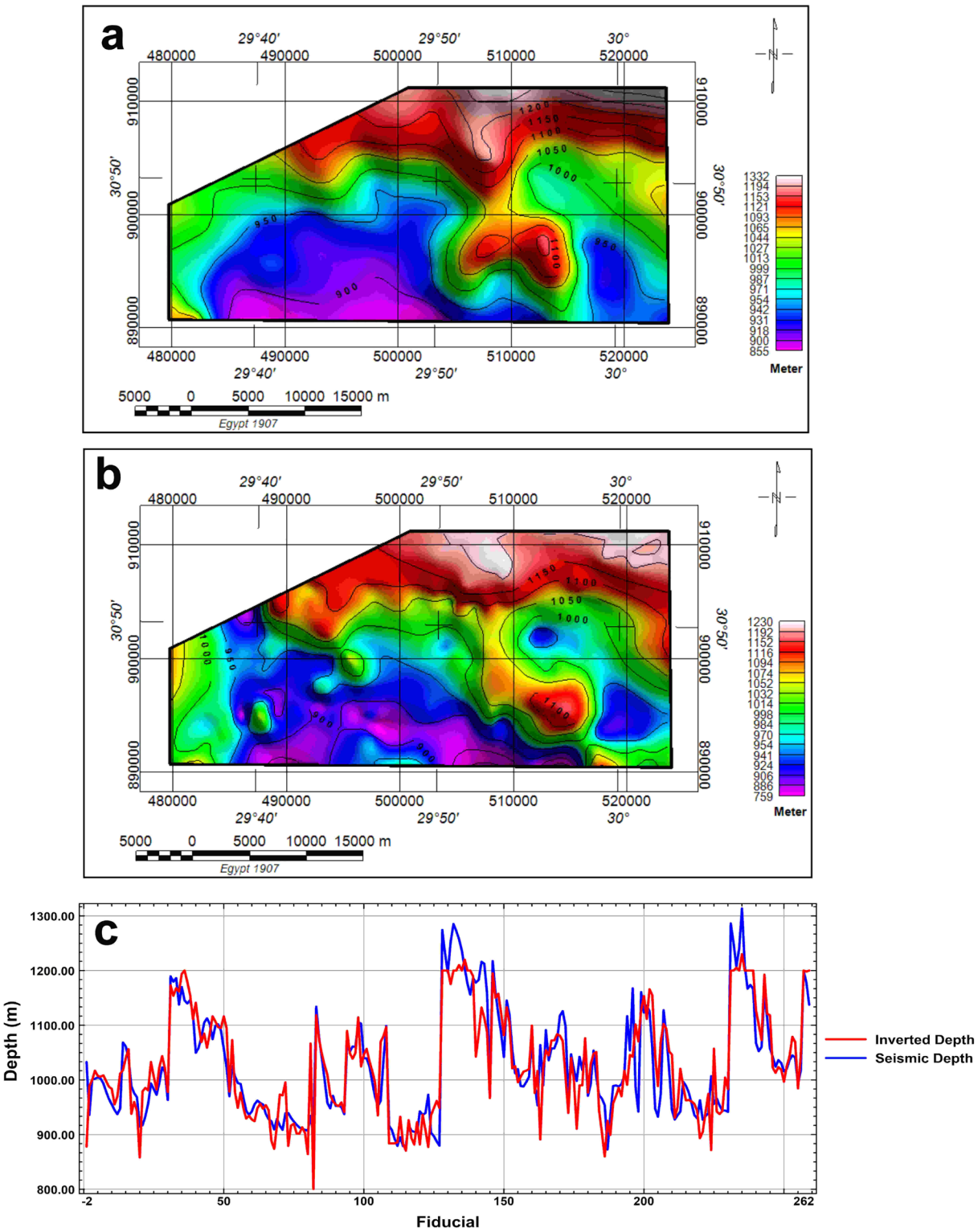

Figure 12. Top Dabaa Formation: (a) Seismic-based depth map; (b) Inverted depth map; (c) Two profiles of the inverted and seismic-based depth. Comparisons between seismic- and gravity-derived depths at all gravity-station locations.

is computed and ranges from −135 to 170.09 m, with a mean difference for the whole map equal to −7.48 m. For a more detailed interpretation of the accuracy of the results, the difference between the two sets of data is constructed in the form of numeric digits and statistically analysed. The least difference between the seismic-based depth and the inverted depth is equal to 0.17 m, which means that the two values of the depths are very close to each other (a good fit between them), where the maximum difference is equal to 170.09 m. The percentage errors

between the two depths are calculated, showing that the percentage error for the top Dabaa Formation ranges from ±0.02 (as a minimum error percentage) to ±16.03% (as a maximum error percentage). A correlation was established between the two depth data sets resulting from gravity data inversion and seismic-based depth to measure their close association and evaluate the strength and direction of linear relationships. The correlation coefficient (R) of the top Dabaa Formation (Fig. 15a) is equal to 0.88, which means that a very strong relationship and closeness of association between the points are found.

The seismic-based depth map of the top Kharita Formation ranges from 2077 to 2809 m (Fig. 13a). The inverted depth map of the top Kharita Formation (Fig. 13b) shows that the depth ranges from 2085 to 2666 m. For the first view, the seismic and inverted-based depth maps (Figs. 13a and 13b) are approximately similar to each other. The northeastern and southern parts are characterized by high depth values ranging from 2400 to 2666 m; the central part is a little bit shallower, and to the west, the depth continues to be shallower, ranging from 2250 to 2085 m. The maximum difference has been found to be equal to 296.06 m; this large difference does not reflect the accuracy of the inverted depth map because the average difference in depth is about 13.08 m for the whole area. The minimum difference is equal to −0.09 m, which means that they have approximately the same depth. The correlation coefficient (R) between the seismic-based depth and the inverted depth (Fig. 15b) is equal to 0.82. This value means a very good relationship between them and a closeness of association between the points. The maximum percentage error for this inverted layer compared to the seismic depth map is equal to ±10.59%.

The top of the El Alamein Formation indicates a relatively shallow depth, reaching 2422 m in the borders of the study area. Conversely, the central part is characterized by a deep depth reaching 3165 m (Fig. 14a). Based on the inverted depth map (Fig. 14b), the depth ranges from 2107 to 3108 m. The inversion findings were subjected to an uncertainty assessment, which revealed an error of approximately ±0.01 to ±21.67%, with a strong correlation between two depth sets of R = 0.75 (Fig. 15c).

The seismic- and gravity-derived depths were compared at every gravity-station location to illustrate their point-by-point correspondence (Figs. 12c, 13c, and 14c). These plots represent station-by-station comparisons rather than continuous physical profiles, which explains the apparent high-frequency variations.

To further validate the inversion results, two representative cross-sections (A-A′ and B-B′) were extracted across the study area (locations shown in Fig. 1). Figure 16 presents a direct comparison between the seismic-based depths and the gravity-inverted depths along these profiles. In both sections, the inverted depths closely follow the seismic depth geometry, with consistent trends and coherent structural behaviour across the three formations. The close alignment of the curves confirms that the apparent high-frequency variations observed in the station-by-station plots (Figs. 12c-14c) do not reflect numerical instability but arise from sequential plotting of discrete gravity-station values. The smoother and geologically consistent behaviour observed along profiles A-A′ and B-B′ strengthens confidence in the inversion workflow and demonstrates that the combined stripping and 3-D inversion approach reliably reproduces independent seismic constraints.

A 2-D model was made using the measured terrestrial gravity data in order to further elucidate the geological structure. The model is established in the NE-SW direction, and its location is shown on the geologic map (Fig. 1). The gravity model response was calculated using GM-SYS (Geosoft, 2008). By reshaping the model or the density of the structural components, the misfit between the measured data and the calculated response of the model is diminished. Updates to the density distribution can force models to be more geologically plausible.

The 2-D model (Fig. 17) extends more than 49 km in the NE-SW direction. The three layers of the top Dabaa, Kharita, and El Alamein Formations were modeled in addition to the basement layer to satisfy the Bouguer gravity profile. The distribution of the assumed density of the blocks of each layer is used to be almost identical to the apparent lateral density distribution used in the 3-D inversion process along the profile. The subsurface is separated into four horizons, each of which is further subdivided into distinct blocks with varying densities. Each single geologic horizon has 100 points that can be moved upward or below to reduce the mismatch between the observed data and the estimated model response.

A minimal misfit between the measured data and the calculated response is achieved by reshaping each layer and adjusting the density. For the basement layer, 2700 kg/m^3 is assumed to be a constant density value. A good match (good fit) between the measured and calculated gravity curves has been observed with a root mean square (RMS) equal to 0.637.

In the 2-D model, assumed densities ranging from 2000 to 2450 kg/m^3 were used for the strata underlying the top Dabaa Formation. Density ranges of 1700 to 2400 kg/m^3 and 1600 to 2450 kg/m^3, respectively, were utilized for the strata underlying the top Kharita and El Alamein Formations.

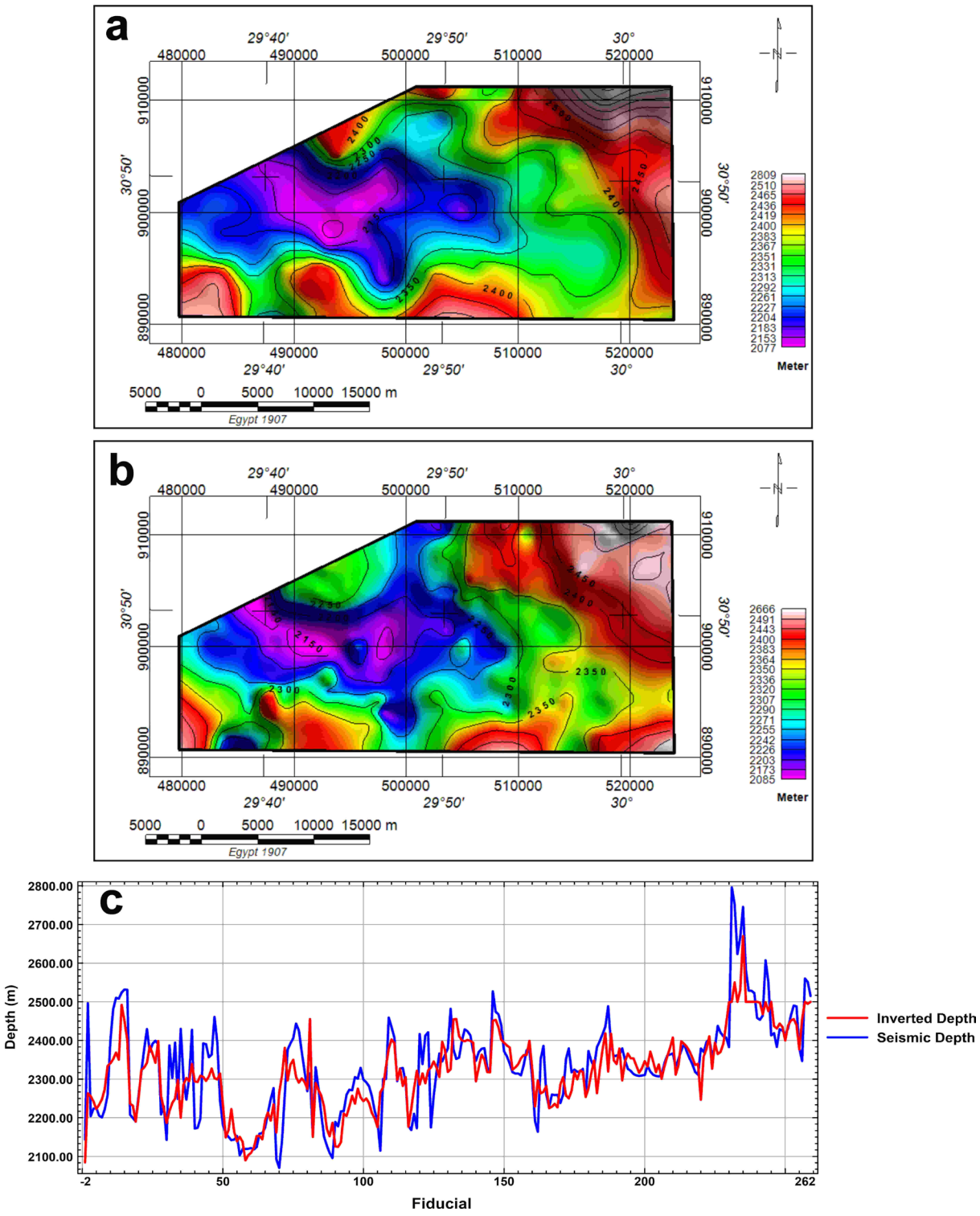

Figure 13. Top Kharita Formation: (a) Seismic-based depth map; (b) Inverted depth map; (c) Two profiles of the inverted and seismic-based depth. . Comparisons between seismic- and gravity-derived depths at all gravity-station locations.

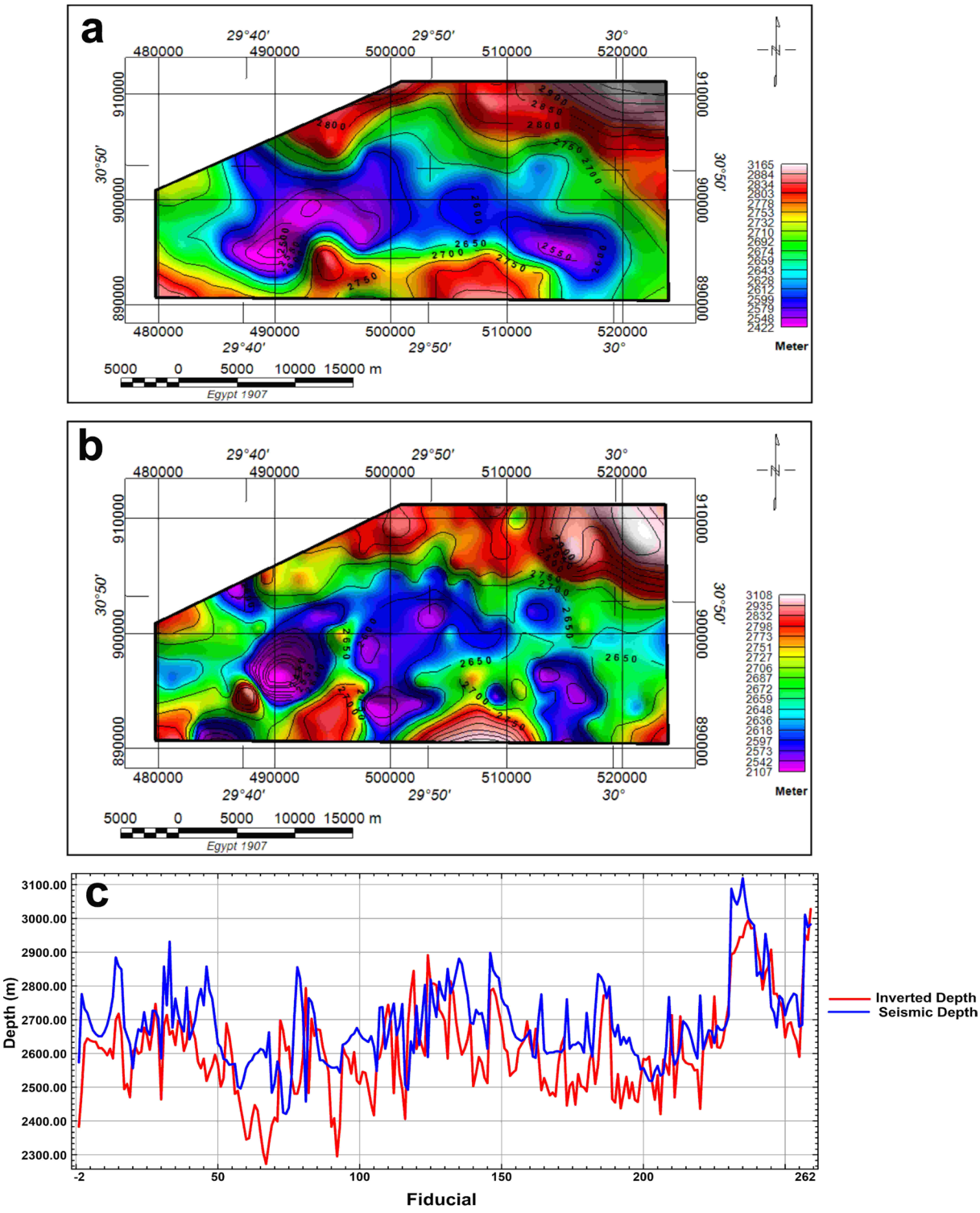

Figure 14. Top El Alamein Formation: (a) Seismic-based depth map; (b) Inverted depth map; (c) Two profiles of the inverted and seismic-based depth. Comparisons between seismic- and gravity-derived depths at all gravity-station locations.

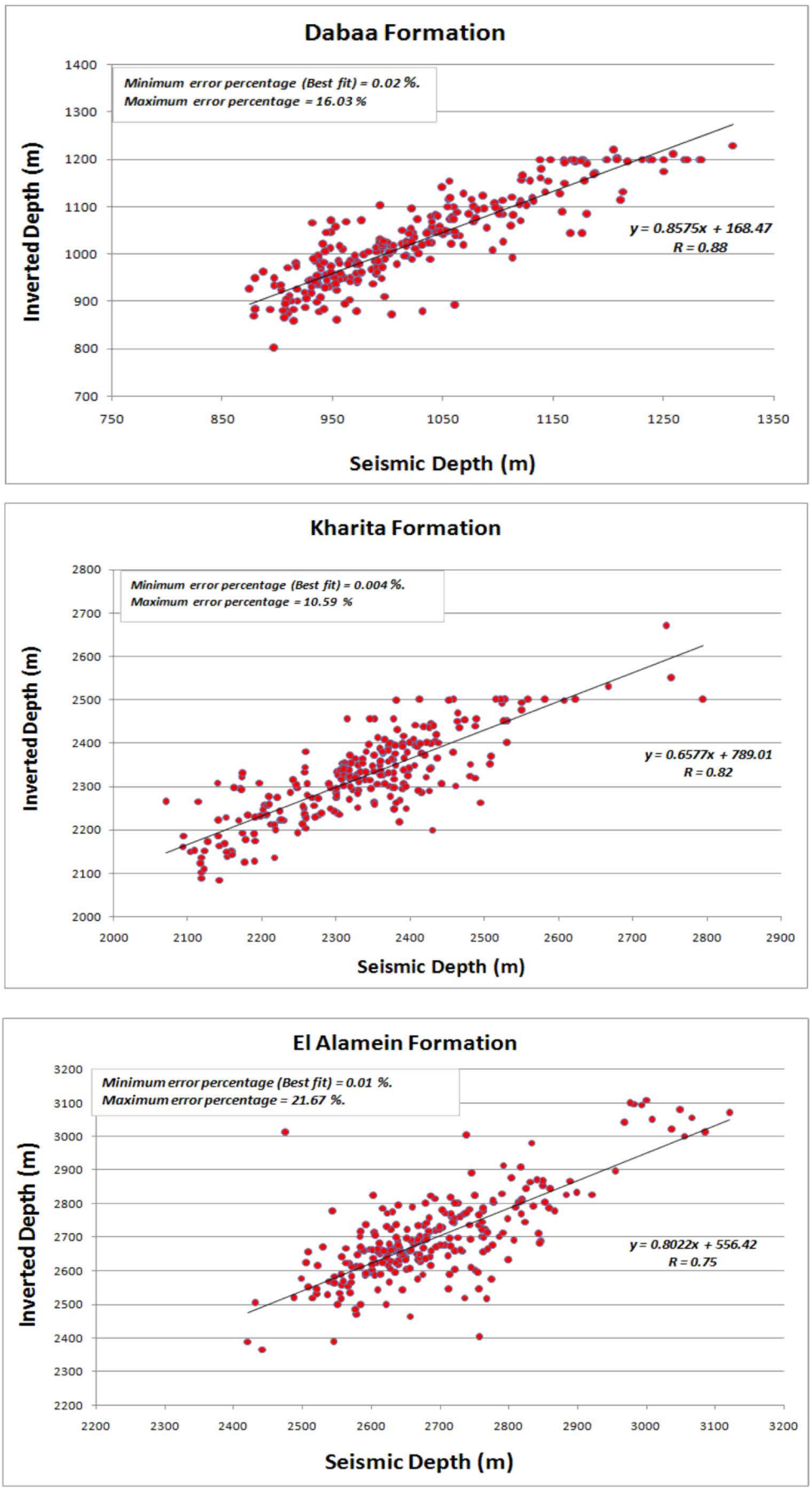

Figure 15. Correlation between the seismic and inverted-based depth of the top: (a) Dabaa; (b) Kharita; (c) El Alamein Formations.

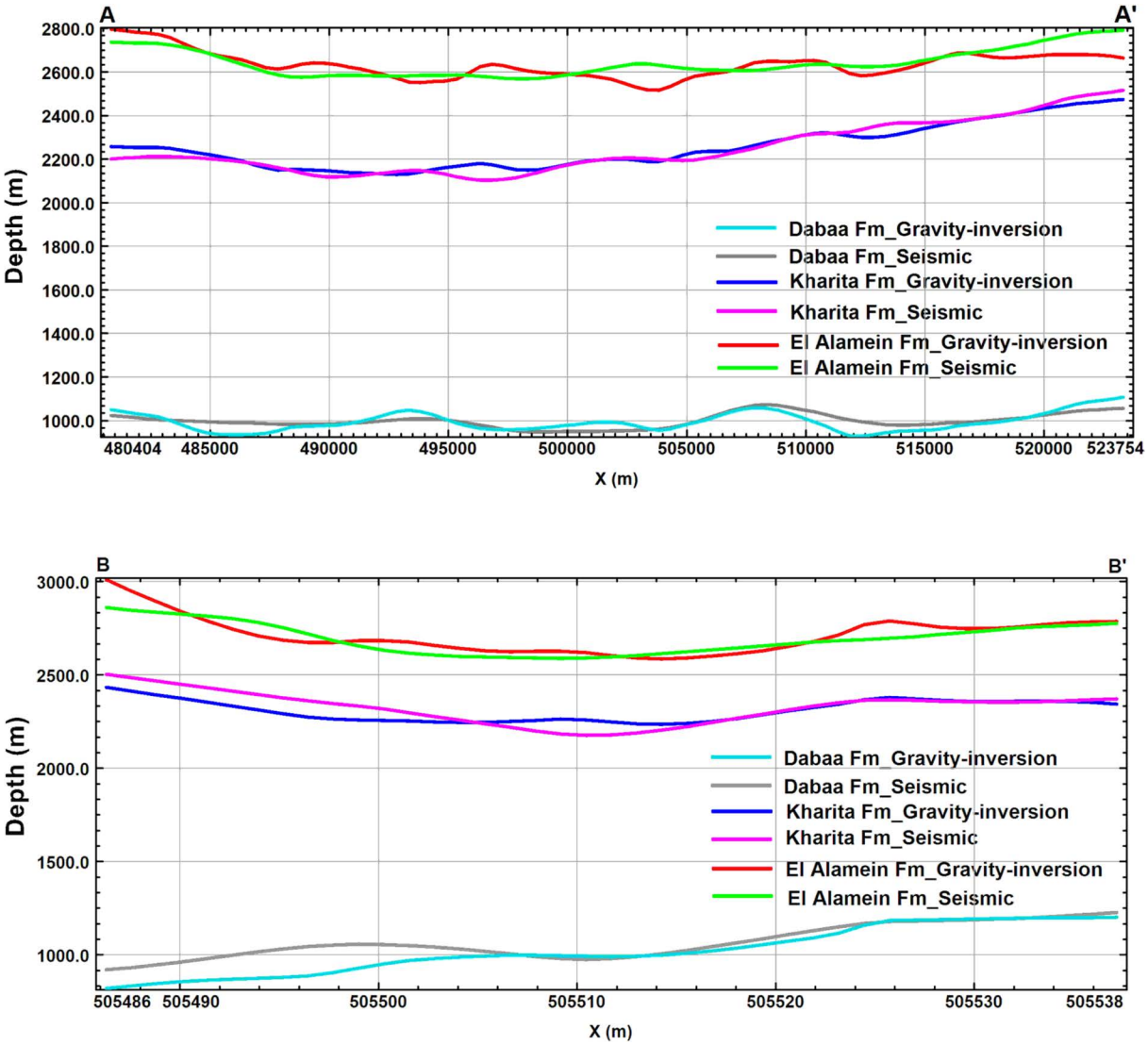

Figure 16. Comparison of seismic-derived and gravity-inverted depths along two representative profiles (A-A′ and B-B′). The profiles illustrate the consistency between the inverted gravity and seismic depths, demonstrating the reliability of the inversion results.

Structurally, the 2-D model shows that the basement layer and the overlying sedimentary succession are affected by a number of normal faults. The depth to the basement layer is about 5600 m and is highly fractured due to a series of normal faults that extend to the upper sedimentary section.

The 2-D model (Fig. 17) shows a series of normal faults that cross most of the model's layers and dip into two directions (SW and NE). The eastern, western, and middle portions of the 2-D model all show significant faults. The 2-D model's normal faults in the east indicate an appropriate displacement of the Dabaa, Kharita, El Alamein, and Basement horizons, which are clearly dipping towards the northeast. The majority of normal faults that dip in the NE direction have a dipping angle ranging from 70° to 80°. In the eastern part of the 2-D model, there are normal faults that have a vertical displacement of around 100 m. Horsts and grabens are formed due to these normal faults. The northeast-southwest extensional system motions in the Early Cretaceous rifting were responsible for the establishment of these faulting directions (Abdel-Fattah et al., 2021; Guiraud and Bosworth, 1997; Moustafa, 2008).

The normal faults dipping in the SW direction have a dipping angle of approximately 75° to 85°. These faults, along with the NE faults, form a number of horsts and grabens. The effect of some normal fault appears on the top Kharita Formation and does not cross the upper section to the top Dabaa Formation.

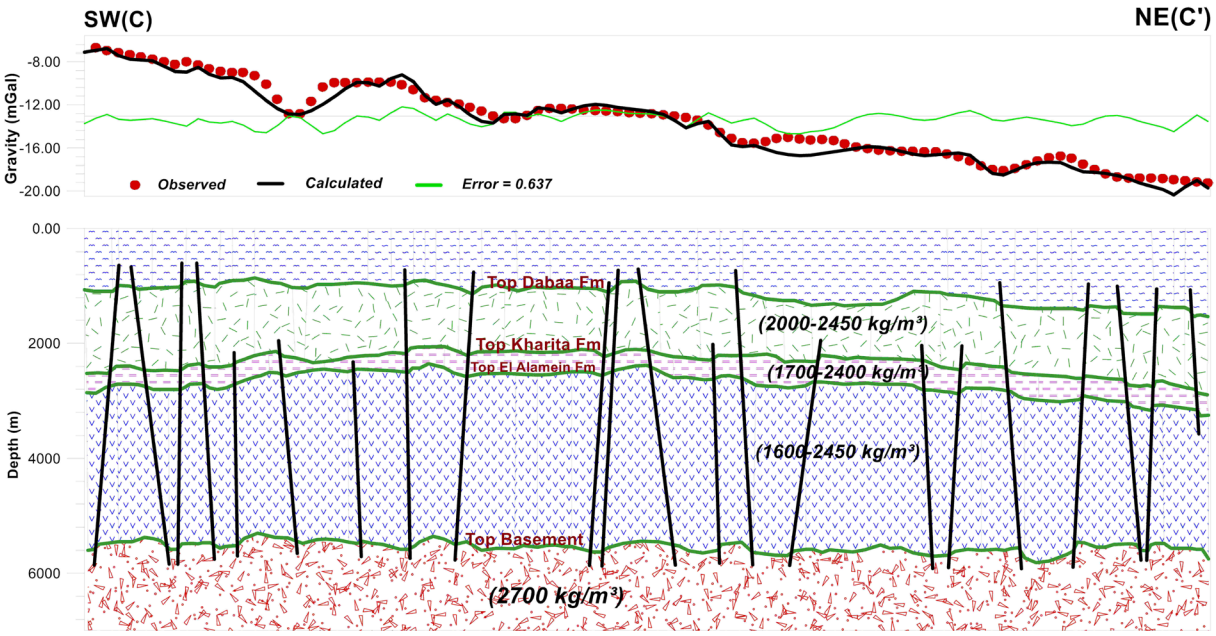

Figure 17. 2-D inverted density layered-earth model along profile C-C′.

6. Conclusion

The gravity method is a geophysical approach that depends on the observed gravity field variations. The measured terrestrial gravity data were measured from 259 stations to determine the variation in gravity field over the Burg EL-Arab area in the Northwestern Desert.

The gravity Bouguer gravity anomaly map (Fig. 3a) was separated using a band-pass filter technique, with $k = 0.05\ km^{-1}$ serving as the cutoff. The regional Bouguer gravity anomaly (Fig. 4a) showed that NE-SW is the dominant trend for long-wavelength anomalies. The first vertical derivative (FVD) of the residual competent (Fig. 5a) showed contact lineaments running NE-SW as the primary trend, in addition to various lineaments exhibiting NNW-SEE and NNE-SSW.

The Bouguer gravity data were separated into three stripped gravity component layers of the top Dabaa, Kharita, and El Alamein Formations (Fig. 10) to achieve the fundamental purpose of this work. Layer-effect grids were analytically estimated from formation thickness and density contrast and assigned to the surface observation level (Bouguer stations) to ensure consistency during stripping. Apparent lateral density distributions for each layer were calculated and used to control gravity data inversion.

The calculated gravity anomaly data and the observed data showed good convergence, with a convergence limit of 0.1 mGal. The performance of the inversion of the terrestrial gravity data is judged by seismic-based depth maps that were generated by the El Paso Company in 2006. The inverted gravity depth maps and the seismic-based depth maps have been found to be very similar. The correlation coefficients (R) between seismic and inverted-based depths for the top Dabaa, Kharita, and El Alamein Formations are 0.88, 0.82, and 0.75, respectively (Fig. 15). Strong associations are shown by the correlation coefficients.

The 2D modeling reveals a series of normal faults in the area, with dipping angles ranging from 70° to 80° in the NE direction and 75° to 85° in the SW direction, forming horsts and grabens. The current study concludes with a proposal that terrestrial gravity data could be used to precisely identify the depth of the sedimentary strata when stripping is performed at the Bouguer-station level and the inversion is constrained by density and seismic information. The maximum tolerance that may be considered is around 21.67%; however, this can be lowered to the minimum error percentage, and sometimes the calculated and actual depths become almost the same value. In conclusion, the gravity data can be highly useful in determining the depth of sedimentary layers when combined with previous knowledge of depth, density, and constrained inversion performance.

Data availability statement. Data is confidential and not for public release.

Acknowledgements. The author expresses his sincere thanks to the Geophysics Department of the Nuclear Material Authority of Egypt for their support in completing this work.

References

Abd El Gawad, E. A., M. Fathy and K. H. Abd El Dayem (2016). Integrated characterization of Desouqy reservoir rock in Faghur-Siwa Basin, Western Desert, Egypt, Int. J. Innov. Sci. Eng. Technol., 3, 24-46, ISSN:2348-7968.

Abdel-Fattah, M., T. Attia, A. Abd El-Aal and M. Hanafy (2021). Seismic interpretation of the Late Albian-Early Cenomanian Bahariya reservoirs of Burg El Arab oil field for tectonic evaluation: a case study from Western Desert, Egypt, Arab. J. Geosci., 14, 412, doi:10.1007/s12517-021-06745-9.

Awad, G. M. (1984). Habitat of oil in Abu Gharadig and Faiyum basins, Western Desert, Egypt, AAPG Bull., 68, 564-573, doi:10.1306/AD46133B-16F7-11D7-8645000102C1865D.

Barbosa, V. C. F., J. B. C. Silva and W. E. Medeiros (1999). Stability analysis and improvement of structural index estimation in Euler deconvolution, Geophysics, 64, 48-60, doi:10.1190/1.1444529.

Beadnell, H. J. L. (1905). The topology and geology of the Fayum Province of Egypt, National Printing Press, Cairo, 1-101.

Blakely, R. J. (1995). Potential theory in gravity and magnetic applications, Cambridge University Press, Cambridge, UK, ISBN:0-521-41508-X.

Bosworth, W., M. Drummond, M. Abrams and M. Thompson (2015). Jurassic rift initiation source rock in the Western Desert, Egypt – relevance to exploration in other continental rift systems, in Petroleum Systems in "Rift" Basins, 34th Annual GCSSEPM Foundation Perkins Rosen Research Conference, GCSSEPM Foundation, Houston, doi:10.5724/gcs.15.34.0615.

Bott, M. H. P. (1963). Two methods applicable to computers for evaluating magnetic anomalies due to finite three-dimensional bodies, Geophys. Prospect., 11, 292-299, doi:10.1111/j.1365-2478.1963.tb02039.x.

Conoco (1987). Geologic map of Egypt, Egyptian General Authority for Petroleum (UNESCO Joint Map Project), Cairo, 20 sheets, scale 1:500,000.

Corbató, C. E. (1965). A least-squares procedure for gravity interpretation, Geophysics, 30, 228-233, doi:10.1190/1.1439560.

Danes, Z. F. (1960). On a successive approximation method for interpreting gravity anomalies, Geophysics, 25, 1215-1228, doi:10.1190/1.1438809.

Edress, N. A., M. S. Fagelnour and M. H. Hassan (2022). Subsurface geology and geochemical evaluation of the Middle Jurassic-Lower Cretaceous organic-rich intervals, West Kalabsha area, Western Desert, Egypt, Arab. J. Geosci., 15, 1401, doi:10.1007/s12517-022-10686-2.

Elmasry, A., M. Abdelzaher, A. Madani and T. Nassar (2022). Exploration of geothermal resources utilizing geophysical and borehole data in the Abu Gharadig Basin of Egypt's Northern Western Desert, Pure Appl. Geophys., 179, 4503-4520, doi:10.1007/s00024-022-03180-z.

Fagelnour, M. S., F. I. Metwalli and E. H. Shendi (2018). Structural and facies modeling of the Lower Cretaceous Alam El Bueib reservoirs in the Shushan Basin, Western Desert, Egypt, Arab. J. Geosci., 11, 1-24, doi:10.1007/s12517-018-3909-4.

Feng, X., S. Liu, R. Guo, P. Wang and J. Zhang (2020). Gravity inversion of blocky basement relief using L_0-norm constraint with exponential density-contrast variation, Pure Appl. Geophys., 177, doi:10.1007/s00024-020-02423-1.

General Petroleum Company (2022). Gravity map of Egypt, General Petroleum Company, Cairo, scale 1:250,000.

Geosoft Inc. (2008). Oasis montaj 7.0 mapping and processing system: the core software platform for working with large-volume spatial data, Geosoft Inc., Ontario.

Guiraud, R. and W. Bosworth (1997). Senonian basin inversion and rejuvenation of rifting in Africa and Arabia: synthesis and implications to plate-scale tectonics, Tectonophysics, 282, 39-82, doi:10.1016/S0040-1951(97)00212-6.

Habeeb, A. H., K. S. Farag and A. M. Abdelaziz (2017). Multi-dimensional inversion of airborne total magnetic intensity data at the West-of-Edfu region, Upper Egypt, IOSR, J. Appl. Geol. Geophys., 5, 1-13, doi:10.9790/0990-0501010113.

Hammer, S. (1963). Deep gravity interpretation by stripping, Geophysics, 28, 369-378, doi:10.1190/1.1439186.

Ismail, I. S., S. A. Saada, Y. M. Y. Ali and Y. M. Y. Ibrahem (2015). An integrated study of gravity and magnetic data to determine subsurface structure and depth to basement in the Alamein area, Western Desert, Egypt, IOSR, J. Appl. Geol. Geophys., 3, 11-29, doi:10.9790/0990-03621129.

Kamal, M., J. Shen, A. A. A. Othamn, S. A. S. Araffa et al. (2023). Integrated geophysical techniques applied for petroleum basins structural characterization in the central part of the Western Desert, Egypt, Open Chem., 21, 20220293, doi:10.1515/chem-2022-0293.

Leeder, M. R. (2011). Sedimentology and sedimentary basins: from turbulence to tectonics, 2nd ed., Wiley-Blackwell, 1328, ISBN:978-1-4443-4992-4.

Lines, L. R. and S. Treitel (1984). A review of least-squares inversion and its application to geophysical problems, Geophys. Prospect., 32, 159-186, doi:10.1111/j.1365-2478.1984.tb00726.x.

Mansour, A., T. Gentzis, M. El Nady, F. Mostafa et al. (2020). Hydrocarbon potential of the Albian-early Cenomanian formations (Kharita-Bahariya) in the North Western Desert, Egypt: a review, J. Petrol. Sci. Eng., 193, 107440, doi:10.1016/j.petrol.2020.107440.

Menke, W. (2012). Geophysical data analysis: discrete inverse theory, 3rd ed., Academic Press, ISBN:9780123977847.

Meshref, W. (1990). Tectonic framework of Egypt, in Geology of Egypt, R. Said (Editor), Balkema, Rotterdam/Brookfield, 113-156.

Milsom, J. (2003). Field geophysics, John Wiley and Sons Ltd., Chichester.

Moustafa, A. R. (2008). Mesozoic-Cenozoic basin evolution in the northern Western Desert of Egypt, in The Geology of East Libya, M. Salem, A. El-Arnauti and A. Saleh (Editors), 3, 29-46.

Norton, P. (1967). Rock stratigraphic nomenclature of the Western Desert, Report of GPC, Cairo, Egypt, 557.

Oldenburg, D. W. (1974). The inversion and interpretation of gravity anomalies, Geophysics, 39, 424-438, doi:10.1190/1.1440444.

Otsuka, T. and K. Ogawa (1977). Combined seismic and gravity interpretation in the West Bakr area, Gulf of Suez, Egypt, Report of Technology Research Center, JPC, Tokyo, 6.

Parasnis, D. S. (2012). Principles of applied geophysics, Springer, Dordrecht, doi:10.1007/978-94-009-5814-2.

Parker, R. L. (1973). The rapid calculation of potential anomalies, Geophys. J. R. Astron. Soc., 31, 447-455, doi:10.1111/j.1365-246X.1973.tb06513.x.

Pilkington, M. and D. J. Crossley (1986). Determination of crustal interface topography from potential fields, Geophysics, 51, 1277-1284, doi:10.1190/1.1442180.

Saada, S. A., A. M. Eldosouky, M. Kamel, A. El Khadragy et al. (2022). Understanding the structural framework controlling the sedimentary basins from the integration of gravity and magnetic data: a case study from the east of the Qattara Depression area, Egypt, J. King Saud Univ. Sci., 34, 101808, doi:10.1016/j.jksus.2021.101808.

Saada, S. A. and A. A. El-Khadragy (2015). An integrated study of gravity and magnetic data on the West El-Minya area, Western Desert, Egypt, Am. J. Sci., 11, 169-184, doi:10.7537/marsjas111215.23.

Said, R. (1962). The geology of Egypt, Elsevier Publishing Co., Amsterdam, Oxford, and New York.

Said, R. (1990). The geology of Egypt, A. A. Balkema, Rotterdam/Brookfield.

Spector, A. and F. S. Grant (1970). Statistical models for interpreting aeromagnetic data, Geophysics, 35, 293-302, doi:10.1190/1.1440092.

Taha, M. A. and M. A. Halim (1992). The impact of sequence stratigraphic synthesis on petroleum exploration in the Western Desert, in Proceedings of the 11th Petroleum Exploration and Production Conference, Cairo, 1988, 2, 39-55.

Tanner, J. G. (1967). An automated method of gravity interpretation, Geophys. J. R. Astron. Soc., 13, 339-347, doi:10.1111/j.1365-246X.1967.tb02164.x.

Tarantola, A. (2005). Inverse problem theory and methods for model parameter estimation, SIAM, Philadelphia.

Webring, M. (1985). A Fortran program for generalized linear inversion of gravity and magnetic profiles, U. S. Geol. Surv. Open-File Rep., 85-122, doi:10.3133/ofr85122.

Xiao, J. (2020). Inverse problems, non-uniqueness and symmetries in geology, PhD thesis, Department of Earth Sciences, Royal Holloway, University of London, 174.

***CORRESPONDING AUTHOR: Hassan MOHAMED**,
Egyptian Nuclear Materials Authority, Ground Geophysics Department, Nuclear Materials Authority, P.O. Box 530, Cairo, Egypt
e-mail: hassan.badr@nma.org.eg